Korean Journal of Chemical Engineering
https://doi.org/10.1007/s11814-024-00239-6

ORIGINAL ARTICLE

# Economic Evaluation of Multi-recycling and Once-Through Fuel Cycle Considering National Plans

**Hong Jang[1] · Hun Suk Im[1] · Jung-ho Hur[1] · Hyo On Nam[1] · Won Il Ko[1]**

Received: 30 March 2024 / Revised: 13 July 2024 / Accepted: 22 July 2024


## Abstract

This paper presents a comparative and quantitative analysis of transition scenarios to potential fuel cycle options, focusing on once-through (OT) and pyro-sodium-cooled fast reactor (pyro-SFR) cycles. By employing a module-based flow diagram in system definition, we developed a dynamic mass-flow model to simulate transition scenarios in line with the current Korean nuclear plans. Additionally, we derived an economic evaluation model to determine the levelized cost of electricity (LCOE) for each fuel cycle option. This model includes detailed equations for calculating reactor capital costs and the optimal concentration of depleted uranium. Our mass-flow analysis highlights the pyro-SFR cycle's superior resource utilization and reduced high-level radioactive waste (HLW) production. However, this cycle necessitates additional reactors and back-end cycle facilities. The economic evaluation reveals a marginally higher LCOE for the pyro-SFR cycle, attributed to the costs of constructing and operating these additional facilities. However, uncertainty analysis indicates that uncertainties in unit costs diminish the impact of the cost difference. Through sensitivity analysis, we identified critical modules and break-even points for unit costs, such as reactor capital and natural uranium mining. Our findings offer crucial insights for decision-making in spent fuel management plans or policies. System analysis always faces challenges due to data limitations and the commercialization barriers of back-end fuel cycle technologies; however, continued efforts to enhance evaluation accuracy and reduce uncertainty are needed.

**Keywords** System analysis · Economic evaluation · Nuclear fuel cycle system · Multi-recycling · Pyro-SFR cycle · Once-through cycle · Levelized cost of electricity · Uncertainty analysis · Sensitivity analysis

## Introduction

Nuclear energy faces obstacles in expanding its share of the energy mix despite its strong economic viability and minimal environmental impact. Decision-making in nuclear energy necessitates a comprehensive evaluation that goes beyond economic and environmental factors. Concerns about the technical feasibility and proliferation resistance of spent fuel management strategies add complexity to the decision-making process, hindering the sustained or increased use of nuclear energy. To effectively tackle these multifaceted problems, system analysis methodologies are essential. System analysis involves comparing alternative options using quantitative evaluation criteria. To quantify these criteria, it is imperative to define the target system options, develop mathematical models, and solve them to determine mass flows. Once the mass flows are established, quantitative criteria, such as resource utilization, environmental impact, and economic viability, can be calculated. An integrated evaluation that considers multiple quantitative criteria simultaneously can then be conducted.

Since its inception in 2000, the International Atomic Energy Agency has initiated the International Project on Innovative Nuclear Reactors and Fuel Cycles (INPRO) to develop system analysis methodologies for nuclear energy systems. INPRO established a toolkit named Analysis Support for Enhanced Nuclear Energy Sustainability (ASENES) [1] to enhance the strategic capabilities of member countries by developing experts proficient in analyzing and evaluating nuclear energy systems and transition scenarios. ASENES comprises four modules. The first module, which includes MESSAGE-NES and NES Simulator, is designed

✉ Hong Jang
janghong@kaeri.re.kr

[1] Korea Atomic Energy Research Institute, 111, Daedeok-daero 989 beon-gil, Yuseong-gu, Daejeon 34057, Republic of Korea

Published online: 05 August 2024

for modeling and analyzing nuclear system transition scenarios. The second module, NEST, assesses the economic feasibility of energy systems. The third module, KIND-ET, aids in comparing and evaluating alternative energy systems and transition scenarios. The fourth module, ROADMAP-ET, focuses on creating roadmaps to improve nuclear energy sustainability. Each module has been validated through multinational projects, such as GAINS, SYNERGIES, KIND, and CENESO [2–5].

Similar to ASENES, the Korea Atomic Energy Research Institute (KAERI) has been advancing system analysis methodologies to quantitatively assess decision-making problems associated with the deployment of nuclear fuel cycle options since 2001. Initially, the period from the early 2000s to the mid-2010s was marked by screening studies that used static system analysis methods to examine various options, including the once-through (OT), DUPIC, MOX, and pyro-SFR cycles [6–12]. The OT cycle is a nuclear fuel cycle that directly disposes of PWR SF. The DUPIC and MOX cycles recycle PWR SF a single time in PHWR and PWR, respectively. And the pyro-SFR cycle recycles PWR SF multiple times in SFR. From the mid-2010s onward, the focus shifted to transition scenario studies employing dynamic system analysis methods for these options [13–16]. As a result of integrated evaluations considering resource utilization, environmental impact, and economic viability, the promising nuclear fuel cycle options in Korea have been narrowed down to the OT and pyro-SFR cycles. Consequently, dynamic system analysis studies for these two cycles have been conducted more intensively [17–19]. Over two decades, KAERI has persistently enhanced and validated its system analysis method, covering mass analysis, economic evaluation, sensitivity and uncertainty analysis, and integrated assessment. With the advent of new input data or changes in national nuclear policies, improved methods were utilized to update the analysis results. Research to refine and develop more robust system analysis methodologies is ongoing.

This paper presents improved mathematical models for conducting mass-flow analysis and economic evaluations of promising fuel cycle options in a well-structured manner. The mass-flow analysis model outlines a clear logic for the transportation of spent fuel to storage and disposal facilities, along with the operation of pyro-processing facility, facilitating the realization of fuel cycle transition scenarios. Furthermore, the economic evaluation model incorporates detailed equations for computing the interest during construction in the reactor cost, and for determining the optimal concentration of depleted uranium aimed at minimizing the front-end fuel cycle cost. In addition, economies of scale have been factored into the unit cost to account for the different scale of the Korean nuclear system compared to the capacity of the reference facility used for unit cost estimation. These refined models for mass-flow analysis and economic evaluation have been validated through comparative analyses of transition scenarios to OT and pyro-SFR cycles, taking into account the current national plans for nuclear energy in Korea.

## System Definition and Modeling

### Definition of Fuel Cycle System Options

Korea operates 22 pressurized water reactors (PWRs) and 3 pressurized heavy water reactors (PHWRs), boasting a total power capacity of 24.7 GWe across the Kori, Saewool, Hanul, Wolsung, and Hanbit sites. As of 2023, these reactors have generated approximately 19,350 tons of spent fuel, which are stored in at-reactor (AR) storage facilities. Approximately 9680 tons of PWR spent fuel are stored in wet storage pools, while approximately 9670 tons of PHWR spent fuel are distributed between wet storage pools and dry storage facilities, such as Silo and MACSTOR. For PHWR spent fuel, seven additional MACSTOR modules have been constructed at the Wolsung site, enhancing the storage capacity to 168,000 assemblies. And for PWR spent fuel, there are also plans to construct AR dry storage facilities at Kori, Hanbit, and Hanul sites. But currently, the wet storage pool at the Kori site is the most saturated, operating at 89% capacity, with the Hanul and Hanbit sites following at 79% capacity. In light of this, there is a urgent need to establish a national strategy for spent fuel management, supported by a system analysis that thoroughly examines and evaluates strategic options.

In this study, the system analysis aims to conduct mass analysis and economic evaluation for the entire lifecycle phases of nuclear energy, employing a methodology akin to lifecycle assessment [20]. The initial step is to define a fuel cycle system that encompasses all lifecycle phases, from uranium mining to radioactive waste disposal. Typically, a fuel cycle system is outlined through a flow diagram. As an exemplary reference, the Idaho National Laboratory (INL) adopted the module concept to articulate a fuel cycle system [21]. Within this framework, a module represents an autonomous yet interdependent facility or service integral to the fuel cycle. This study evaluated two fuel cycle options: the OT cycle and the multi-recycling cycle via pyro-processing in conjunction with an SFR, for spent fuel management. Pyro-processing is a technique for recovering fuel elements from spent fuel using an electrochemical method in molten salt. Recycling fuel elements in SFR fuels can notably reduce the volume, long-term heat load, and radiotoxicity of HLW [22]. The system's definition, utilizing INL modules, is depicted in Fig. 1.

The front-end cycle of the OT cycle for the PWR Reactor (R1) includes the Natural Uranium Mining and Milling (A1), Conversion (B), Enrichment (C1), Fuel Fabrication

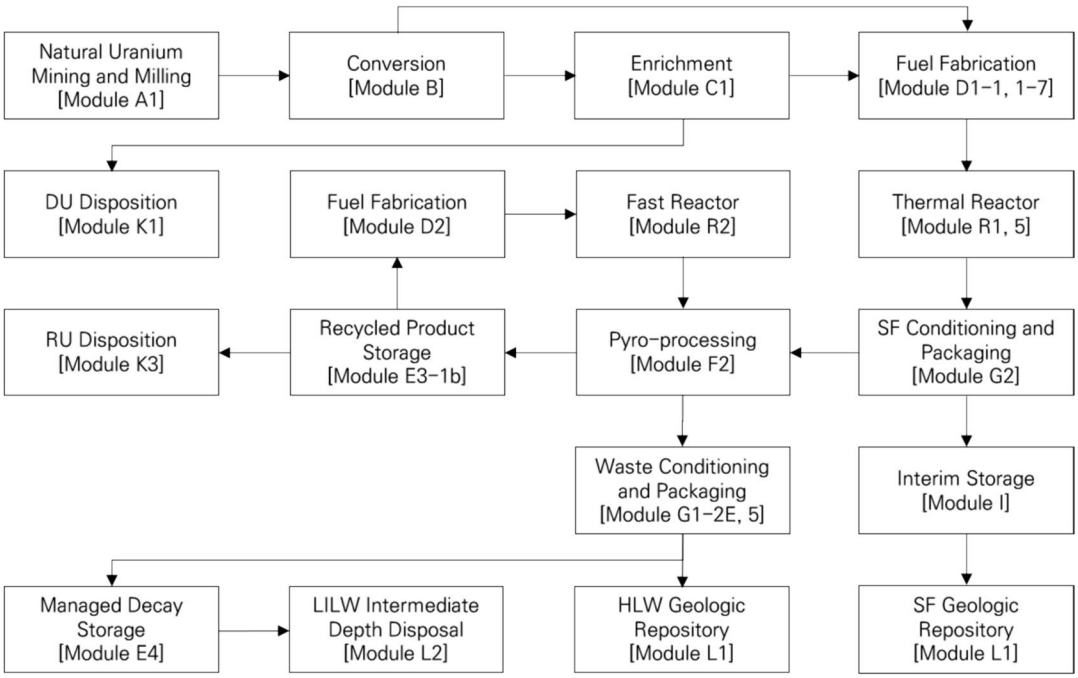


**Fig. 1** Fuel cycle system definition based on INL module concept

(D1–1, 1–7, 2), and DU (depleted uranium) Disposition (K1) modules. And the back-end cycle includes the SF (spent fuel) Conditioning and Packaging (G2), Interim Storage (I), and SF Geologic Repository (L1) modules. For the pyro-SFR cycle, associated with both the PWR Reactor (R1) and the Fast Reactor (R2), the front-end cycle is the same with the OT cycle. However, the back-end cycle diverges significantly. It comprises the SF Conditioning and Packaging (G2), Pyro-processing (F2), Recycled Product Storage (E3-1b), RU (recovered uranium) Disposition (K3), Waste Conditioning and Packaging (G1-2E, 5), Managed Decay Storage (E4), HLW Geologic Repository (L1), and LILW (low and intermediate-level waste) Intermediate Depth Disposal (L2) modules.

The front-end cycle of the OT cycle for the PHWR Reactor (R5) includes the Natural Uranium Mining and Milling (A1), Conversion (B), and Fuel Fabrication (D1-7) modules. The back-end cycle includes the SF Conditioning and Packaging (G2), Monitored Retrievable Storage (I), and SF Geologic Repository (L1) modules. Recycling of PHWR spent fuels was not considered in this work.

## Mass Flow Model

The mass-flow model for the fuel cycle system is predicated on the assumption of a static and continuous state, where all mass flows within the system are constant over time and occur simultaneously. This model utilizes mass balance equations for major groups of radionuclides, including uranium isotope (U), transuranic element (TRU), and fission product (FP). However, given the dynamic nature of reactor operation scenarios that align with national plans, power generation capacity is subject to fluctuation over time. This results in variations in the amounts of fresh fuel loaded, spent fuel generated, and mass flows propagated to the front- and back-end cycles. To address this, a dynamic mass-flow model was developed. It relies on mass balance equations and assumes a static and continuous state for each annual time step, with changing masses of fresh and spent fuels. The calculations for power capacity, serving as the foundation for mass-flow calculations, are as follows:

$$P_i^t = P_{i,his}^t + P_{i,new}^t, \tag{1}$$

$$P_{i,his}^{t_0} = P_{i,his,current}, \tag{2}$$

$$P_{i,his}^t = P_{i,his}^{t-1} - P_{i,his,decom}^{t-1}, \tag{3}$$

$$P_{i,new}^t = P_{i,new}^{t-1} + P_{i,new,com}^{t-1} - P_{i,new,decom}^{t-1}, \tag{4}$$

$$P_{i,decom}^t = P_{i,his,decom}^t + P_{i,new,decom}^t, \tag{5}$$

where $P_i^t$, $P_{i,his}^t$, and $P_{i,new}^t$ denote the total power capacity of reactor $i$ at time $t$, the total power capacity of historical reactor $i$ at time $t$ and the total power capacity of new reactor $i$ at time $t$ built after the reference point $t_0$, respectively, and $P_{i,his,current}$ represents the total power capacity of historical

reactor $i$ at reference point $t_0$. $P^t_{i,his,decom}$ signifies the total power capacity of the historical reactor $i$ decommissioned at time $t$, and $P^t_{i,new,com}$ and $P^t_{i,new,decom}$ denote the total power capacities of the new reactor $i$ commissioned and decommissioned at time $t$, respectively. $P^t_{i,decom}$ stands for the total power capacity of reactor $i$ decommissioned at time $t$.

The mass-flow calculation equations for the Fuel Fabrication (D1-1, 1-7) module are as follows:

$$M^t_{i,FF} = M^t_{i,FF,annual} + M^t_{i,FF,initial}, \tag{6}$$

$$M^t_{i,FF,annual} = \frac{P^t_i \times CF_i \times 365}{BU_i \times Eff_i}, \tag{7}$$

$$M^t_{i,FF,initial} = \frac{P^{t-1}_{i,new,com} \times RT_i - P^{t-1}_{i,new,com} \times CF_i \times 365}{BU_i \times Eff_i}, \tag{8}$$

where $M^t_{i,FF}$, $M^t_{i,FF,annual}$, and $M^t_{i,FF,initial}$ denote the total, annual and initial amounts of fresh fuel fabricated for the operation of reactor $i$ at time $t$, respectively. $CF_i$, $BU_i$, $Eff_i$, and $RT_i$ denote the capacity factor, average burn-up, thermal efficiency, and residence time of the reactor $i$, respectively.

The mass-flow calculation equations for the National Uranium Mining and Milling (A1), Conversion (B), Enrichment (C1), and DU Disposition (K1) modules are as follows:

$$M^t_{i,EU} = M^t_{i,FF}, \tag{9}$$

$$M^t_{i,NU} = M^t_{i,EU} + M^t_{i,DU}, \tag{10}$$

$$M^t_{i,NU} \times x_{i,NU} = M^t_{i,EU} \times x_{i,EU} + M^t_{i,DU} \times x_{i,DU}, \tag{11}$$

$$M^t_{i,Conv} = M^t_{i,NU}, \tag{12}$$

$$M^t_{i,SWU} = M^t_{i,EU} \times X_{i,EU} + M^t_{i,DU} \times X_{i,DU} - M^t_{i,NU} \times X_{i,NU}, \tag{13}$$

$$X_{i,NU} = \left(2x_{i,NU} - 1\right) \times \ln\left(\frac{x_{i,NU}}{1 - x_{i,NU}}\right), \tag{14}$$

$$X_{i,EU} = \left(2x_{i,EU} - 1\right) \times \ln\left(\frac{x_{i,EU}}{1 - x_{i,EU}}\right), \tag{15}$$

$$X_{i,DU} = \left(2x_{i,DU} - 1\right) \times \ln\left(\frac{x_{i,DU}}{1 - x_{i,DU}}\right), \tag{16}$$

$$M^t_{i,DU,accumul} = M^{t-1}_{i,DU,accumul} + M^{t-1}_{i,DU}, \tag{17}$$

where $M^t_{i,NU}$, $M^t_{i,EU}$, and $M^t_{i,DU}$ denote the mass flows of the natural uranium (NU) mined, enriched uranium (EU) produced, and DU generated for the operation of reactor $i$ at time $t$, respectively. $x_{i,NU}$, $x_{i,EU}$, and $x_{i,DU}$ represent the $^{235}$U composition in NU, EU, and DU, respectively, for the operation of reactor $i$. $M^t_{i,Conv}$ and $M^t_{i,SWU}$ denote the conversion mass flow and separate work units, respectively, for the operation of reactor $i$ at time $t$. In the case of the PHWR, where the EU is not used, $x_{i,EU}$ is the same as $x_{i,NU}$ and $x_{i,DU}$ is 0. $M^t_{i,DU,accumul}$ signifies the accumulative mass flow of the DU generated for the operation of reactor $i$ at time $t$.

The equations for calculating the amount of spent fuels generated are as follows:

$$M^t_{i,SF} = M^t_{i,SF,annual} + M^t_{i,SF,final}, \tag{18}$$

$$M^t_{i,SF,annual} = M^t_{i,FF,annual}, \tag{19}$$

$$M^t_{i,SF,final} = \frac{P^{t-1}_{i,decom} \times RT_i - P^{t-1}_{i,decom} \times CF_i \times 365}{BU_i \times Eff_i}, \tag{20}$$

$$M^t_{i,SF,accumul} = M^{t-1}_{i,SF,accumul} + M^{t-1}_{i,SF}, \tag{21}$$

$$M^{t_0}_{i,SF} = M_{i,SF,current}, \tag{22}$$

where $M^t_{i,SF}$, $M^t_{i,SF,annual}$, and $M^t_{i,SF,final}$ denote the total, annual, and final amounts of spent fuels generated from reactor $i$ and stored in reactor $i$ at time $t$, respectively. $M^t_{i,SF,accumul}$ represents the accumulative mass flow of spent fuels generated from reactor $i$ at time $t$, and $M_{i,SF,current}$ signifies the current amount of spent fuels generated from reactor $i$ before the reference point $t_0$.

The mass-flow calculation equations for the SF Conditioning and Packaging (G2), Monitored Retrievable Storage (I), and SF Geologic Repository (L1) modules in the OT cycle are as follows:

$$M^t_{i,SFcond} = M^{t-T_{i,SF,cool}}_{i,SF}, \tag{23}$$

$$M^t_{i,IS} = M^t_{i,SFcond}, \tag{24}$$

$$M^t_{i,SFdis} = M^{t-T_{i,SF,sto}}_{i,IS}, \tag{25}$$

$$M^t_{i,IS,accumul} = M^{t-1}_{i,IS,accumul} + M^{t-1}_{i,IS} - M^{t-1}_{i,SFdis}, \tag{26}$$

$$M^t_{i,SFdis,accumul} = M^{t-1}_{i,SFdis,accumul} + M^{t-1}_{i,SFdis}, \tag{27}$$

where $M^t_{i,SFcond}$, $M^t_{i,IS}$, and $M^t_{i,SFdis}$ denote the mass flows of conditioning and packaging, interim storage, and disposal of the spent fuel of reactor $i$ at time $t$, respectively. $M^t_{i,IS,accumul}$ and $M^t_{i,SFdis,accumul}$ represent the accumulative mass flows of interim storage and disposal of the spent fuel of reactor $i$ at time $t$. $T_{i,SF,cool}$ and $T_{i,SF,sto}$ denote the required cooling time for transportation and storage time for disposal of the spent fuel of reactor $i$.

If a specific point in time is identified for securing the interim storage facility, mass flow to this facility cannot occur before that time, even if the required cooling time for transportation has been met. Consequently, the transport logic for directing mass flow to the interim storage facility must be incorporated into Eq. (24) as follows:

$$\begin{cases} M^t_{i,IS} = 0, M^{T_{IS,oper}}_{i,IS} = M^{T_{IS,oper}}_{i,IS} + M^{t-T_{i,SF,cool}}_{i,SF} & \text{for } t \le T_{IS,oper} \\ M^t_{i,IS} = M^{t-T_{i,SF,cool}}_{i,IS} & \text{for } t > T_{IS,oper} \end{cases}, \tag{28}$$

where $T_{IS,oper}$ denotes the time at which the interim storage facility is secured. If there is a limit on the annual transport mass to the interim storage facility, the transport logic can be added as follows:

$$\begin{cases} M^{t+1}_{i,IS} = M^{t+1}_{i,IS} + \left(M^t_{i,IS} - M_{i,IS,max}\right) & \text{for } M^t_{i,IS} > M_{i,IS,max}, \\ M^t_{i,IS} = M_{i,IS,max} \end{cases} \tag{29}$$

where $M_{i,IS,max}$ represents the limit of the annual transport mass to the interim storage facility for the spent fuel in reactor $i$.

Similarly, if a specific point in time at which the final disposal facility is secured is determined, the mass flow to the disposal facility cannot exist before that point, even if the required storage time for disposal is satisfied. In this case, the transport logic for the mass flow to the disposal facility should be added to Eq. (25), as follows:

$$\begin{cases} M^t_{i,SFdis} = 0, M^{T_{SFdis,oper}}_{i,SFdis} = M^{T_{SFdis,oper}}_{i,SFdis} + M^{t-T_{i,SF,sto}}_{i,IS} & \text{for } t \le T_{SFdis,oper} \\ M^t_{i,SFdis} = M^{t-T_{i,SF,sto}}_{i,IS} & \text{for } t > T_{SFdis,oper} \end{cases}, \tag{30}$$

where $T_{SFdis,oper}$ denotes the time at which the disposal facility is secured. If there is a limit on the annual transport mass to the final disposal facility, the transport logic can be added as follows:

$$\begin{cases} M^{t+1}_{i,SFdis} = M^{t+1}_{i,SFdis} + \left(M^t_{i,SFdis} - M_{i,SFdis,max}\right) & \text{for } M^t_{i,SFdis} > M_{i,SFdis,max}, \\ M^t_{i,SFdis} = M_{i,SFdis,max} \end{cases} \tag{31}$$

where $M_{i,SFdis,max}$ represents the limit of the annual transport mass to the final disposal facility for the spent fuel in reactor $i$.

The mass-flow calculation equation for the SF Conditioning and Packaging (G2) module in the pyro-SFR cycle is the same with Eq. (23). The equations for calculating mass flow of the Monitored Retrievable Storage (I) and Pyro-processing (F2) modules in the pyro-SFR cycle are as follows:

$$M^t_{i,IS,accumul} = M^{t-1}_{i,IS,accumul} + M^{t-1}_{i,IS} - M^{t-1}_{i,SFdis} - M^{t-1}_{i,Pyro}, \tag{32}$$

$$M^t_{PWR,Pyro} = \min\left(\frac{M^t_{SFR,FF} \times x_{SFR,fuel,TRU}}{x_{PWR,SF,TRU}}, M^t_{PWR,IS,accumul}\right), \tag{33}$$

$$M^t_{SFR,Pyro} = \min\left(\frac{M^t_{SFR,FF} \times x_{SFR,fuel,TRU} - M^t_{PWR,Pyro} \times x_{PWR,SF,TRU}}{x_{SFR,SF,TRU}}, M^t_{SFR,IS,accumul}\right), \tag{34}$$

where $M^t_{i,Pyro}$ denotes the pyro-processing mass flow for the spent fuel of reactor $i$ at time $t$. $x_{SFR,fuel,TRU}$ denotes the TRU composition of the SFR fresh fuel, and $x_{i,SF,TRU}$ represents the TRU composition of the spent fuel of reactor $i$. In the pyro-processing facility, spent fuel undergoes processing to extract only the amount of TRU required for SFR operation. By adopting this approach, the accumulation of plutonium can be effectively managed. Initially, TRUs are extracted from the PWR SF. Once the TRUs from PWR spent fuel have been depleted, the process then shifts to extracting TRUs from SFR spent fuel.

The mass-flow calculation equations for the Recycled Product Storage (E3-1b) and RU Disposition (K3) modules are as follows:

$$M^t_{i,TRU} = M^t_{i,Pyro} \times x_{i,SF,TRU}, \tag{35}$$

$$M^t_{i,TRU,accumul} = M^{t-1}_{i,TRU,accumul} + M^{t-1}_{i,TRU} - M^{t-1}_{SFR,FF} \times x_{SFR,fuel,TRU}, \tag{36}$$

$$M^t_{i,RU} = M^t_{i,Pyro} \times x_{i,SF,U}, \tag{37}$$

$$M^t_{i,RU,accumul} = M^{t-1}_{i,RU,accumul} + M^{t-1}_{i,RU} - M^{t-1}_{SFR,FF} \times x_{SFR,fuel,U}, \tag{38}$$

where $M^t_{i,TRU}$ and $M^t_{i,TRU,accumul}$ denote the mass flow and accumulative mass flow of TRU separated from the pyro-processing of the spent fuel of reactor $i$ at time $t$, and $M^t_{i,RU}$ and $M^t_{i,RU,accumul}$ represent the mass flow and accumulative mass flow of recovered U (RU) separated from the

pyro-processing of the spent fuel of reactor $i$ at time $t$. Further, $x_{SFR,fuel,U}$ denotes the U composition in the SFR fresh fuel.

The equations for calculating mass flow of the Waste Conditioning and Packaging (G1-2E, G5), Managed Decay Storage (E4), HLW Deep Geologic Repository (L1), and Intermediate Depth Disposal (L2) modules are as follows:

$$M^t_{i,HLWdis} = M^t_{i,Pyro} \times x_{i,SF,HLW}, \tag{39}$$

$$M^t_{i,HLWdis,accumul} = M^{t-1}_{i,HLWdis,accumul} + M^{t-1}_{i,HLWdis}, \tag{40}$$

$$M^t_{i,LILWdis} = M^{t-1}_{i,Pyro} \times x_{i,SF,LILW}, \tag{41}$$

$$M^t_{i,LILWdis,accumul} = M^{t-1}_{i,LILWdis,accumul} + M^{t-1}_{i,LILWdis}, \tag{42}$$

$$M^t_{i,LILWcond} = M^t_{i,LILWdis}, \tag{43}$$

$$M^t_{i,Decay} = M^t_{i,Pyro} \times x_{i,SF,Decay}, \tag{44}$$

$$M^t_{i,Decay,accumul} = M^{t-1}_{i,Decay,accumul} + M^{t-1}_{i,Decay}, \tag{45}$$

$$M^t_{i,HLWcond} = M^t_{i,HLWdis} + M^t_{i,Decay}, \tag{46}$$

where $M^t_{i,HLWdis}$ and $M^t_{i,HLWdis,accumul}$ denote the mass flow and accumulative mass flow of disposal of HLW generated from pyro-processing of the spent fuel of reactor $i$ at time $t$. $M^t_{i,LILWdis}$ and $M^t_{i,LILWdis,accumul}$ represent the mass flow and accumulative mass flow of disposal, and $M^t_{i,LILWcond}$ signifies the mass flow of conditioning and packaging of LILW from pyro-processing of the spent fuel of reactor $i$ at time $t$. $M^t_{i,Decay}$ and $M^t_{i,Decay,accumul}$ signify the mass flow and accumulative mass flow of decay storage of high heat-emitting radioactive waste from pyro-processing of the spent fuel of reactor $i$ at time $t$. $x_{i,SF,HLW}$, $x_{i,SF,LILW}$, and $x_{i,SF,Decay}$ denote the waste generation ratios of HLW, LILW, and high heat-emitting radioactive waste, respectively. $M^t_{i,HLWcond}$ represents the mass flow of the conditioning and packaging of HLW generated from pyro-processing of the spent fuel of reactor $i$ at time $t$.

## Economic Evaluation Model

The economic evaluation hinges on the LCOE, calculated by dividing the total present value of costs incurred for power generation by the total present value of electricity generated. This method is particularly useful for comparing fuel cycle system options with different total power generation capacities. The equations for calculating the LCOE of the fuel cycle system are as follows:

$$C_{LCOE} = \frac{\sum_t C^t_{PV}}{\sum_t E^t_{PV}}, \tag{47}$$

$$C^t_{PV} = C^t_{FV} \times (1+r)^{t_0-t}, \tag{48}$$

$$E^t_{PV} = E^t_{FV} \times (1+r)^{t_0-t}, \tag{49}$$

$$C^t_{FV} = C^t_{Capital} + C^t_{O\&M} + C^t_{FC}, \tag{50}$$

$$E^t_{FV} = \sum_i P^t_i \times CF_i \times 365 \times 24, \tag{51}$$

where $C_{LCOE}$ denotes the LCOE of the fuel cycle system, and $C^t_{PV}$ and $E^t_{PV}$ represent the present values of the total cost and electricity generation at time $t$, respectively, and $C^t_{FV}$ and $E^t_{FV}$ denote the future values of the total cost and electricity generation at time $t$. $C^t_{Capital}$, $C^t_{O\&M}$, and $C^t_{FC}$ signify the costs of reactor capital, reactor operation and maintenance (O&M), and fuel cycle at time $t$, respectively. And $r$ denotes the real discount rate.

The reactor capital cost represents the most significant portion of the total cost. In general, the equation to calculate reactor capital cost incorporates interest during both construction and operation, as follows:

$$C^t_{Capital} = \sum_i \left\{ P^t_i \times C_{i,UC,OC} \times \left(1 - IDC_i\right) \times CRF_i \right\}, \tag{52}$$

$$CRF_i = \frac{R}{1-(1+R)^{-T_{i,Life}}}, \tag{53}$$

where $C_{i,UC,OC}$ represents the unit cost of reactor overnight capital for reactor $i$, and $IDC_i$ denotes the interest during construction for reactor $i$, and $CRF_i$ denotes the capital recovery factor for reactor $i$. $R$ and $T_{i,Life}$ represent the interest rate and lifespan of reactor $i$. The investment model with an S-curve and $IDC_i$ calculation equation from the investment model are as follows:

$$\begin{cases} F^{\hat{t}}_{i,inv,accumul} = \frac{9}{4}\left(\hat{t}/T_{i,const}\right)^2 & \text{for } 0 \le \left(\hat{t}/T_{i,const}\right) \le \frac{1}{3} \\ F^{\hat{t}}_{i,inv,accumul} = \frac{3}{2}\left(\hat{t}/T_{i,const}\right) - \frac{1}{4} & \text{for } \frac{1}{3} \le \left(\hat{t}/T_{i,const}\right) \le \frac{2}{3} \\ F^{\hat{t}}_{i,inv,accumul} = \frac{9}{2}\left(\hat{t}/T_{i,const}\right) - \frac{9}{4}\left(\hat{t}/T_{i,const}\right)^2 - \frac{5}{4} & \text{for } \frac{2}{3} \le \left(\hat{t}/T_{i,const}\right) \le 1 \end{cases}, \tag{54}$$

$$IDC_i = \sum_{\hat{t}=1}^{T_{i,const}} \left\{ \left( F^{\hat{t}}_{i,inv,accumul} - F^{\hat{t}-1}_{i,inv,accumul} \right) \times \left[ \left( 1 + \frac{R}{12} \right)^{T_{i,const}-\hat{t}} - 1 \right] \right\}, \tag{55}$$

where $F^{\hat{t}}_{i,inv,accumul}$ represents the accumulated investment fraction of the reactor overnight capital cost for reactor $i$ at monthly time $\hat{t}$, and $T_{i,const}$ is the construction period for reactor $i$.

The calculation equation for the reactor O&M cost is as follows:

$$C_{O\&M} = \sum_i \left\{ P^t_i \times C_{i,UC,O\&M,fix} + E^t_{i,FV} \times C_{i,UC,O\&M,var} \right\}, \tag{56}$$

where $C_{i,UC,O\&M,fix}$ and $C_{i,UC,O\&M,var}$ denote the unit costs of the fixed and variable components of reactor O&M for reactor $i$, respectively.

The calculation equation for the fuel cycle cost is as follows:

$$C^t_{FC} = C^t_{FC,FE} + C^t_{FC,BE}, \tag{57}$$

where $C^t_{FC,FE}$ and $C^t_{FC,BE}$ represent the fuel cycle costs expended in the front-end (FE) and back-end (BE) cycles at time $t$.

The calculation equations for the FE fuel cycle cost are as follows:

$$C^t_{FC,FE} = C^t_{NU} + C^t_{Conv} + C^t_{Enr} + C^t_{DU} + C^t_{FF}, \tag{58}$$

$$C^t_{NU} = \sum_i \left( M^t_{i,NU} \times C_{UC,NU} \right), \tag{59}$$

$$C^t_{Conv} = \sum_i \left( M^t_{i,Conv} \times C_{UC,Conv} \right), \tag{60}$$

$$C^t_{Enr} = \sum_i \left( M^t_{i,SWU} \times C_{UC,Enr} \right), \tag{61}$$

$$C^t_{DU} = \sum_i \left( M^t_{i,DU} \times C_{UC,DU} \right), \tag{62}$$

$$C^t_{FF} = \sum_i \left( M^t_{i,FF} \times C_{i,UC,FF} \right), \tag{63}$$

where $C^t_{NU}$, $C^t_{Conv}$, $C^t_{Enr}$, $C^t_{DU}$, and $C^t_{FF}$ represent the costs expended on the NU mining and milling, conversion, enrichment, DU disposal, and fuel fabrication at time $t$, respectively. $C_{UC,NU}$, $C_{UC,Conv}$, $C_{UC,Enr}$, and $C_{UC,DU}$ denote the unit costs of the NU mining and milling, conversion, enrichment, and DU disposition, respectively, and $C_{i,UC,FF}$ denotes the unit cost of fuel fabrication for reactor $i$.

For the given values of $C_{UC,NU}$, $C_{UC,Conv}$, $C_{UC,Enr}$, and $C_{UC,DU}$, the optimal amount of SWU that minimizes the FE fuel cycle cost can be derived. The amount of SWU, $M^t_{i,SWU}$ is usually determined using $x_{DU}$, because $x_{NU}$ and $x_{EU}$ for the PWR are fixed, as shown in Eq. (13). Simultaneously, the mass flows, $M^t_{i,NU}$, $M^t_{i,Conv}$, and $M^t_{i,DU}$ are determined using Eq. (10)–(12). Therefore, the optimization problem for determining the optimal $x_{DU}$ that minimizes the FE fuel cycle cost is defined as follows:

$$\min_{x_{DU}} \left( M^t_{PWR,NU} \times C_{UC,NU} + M^t_{PWR,Conv} \times C_{UC,Conv} + M^t_{PWR,SWU} \times C_{UC,Enr} + M^t_{PWR,DU} \times C_{UC,DU} \right). \tag{64}$$

After substituting Eqs. (10)–(16) into the objective function, a simplified objective function independent of the mass flow can be derived as follows:

$$\min_{x_{DU}} \left( \frac{P + X_{DU} - X_{NU}}{x_{NU} - x_{DU}} \right), \tag{65}$$

$$P = \frac{C_{UC,NU} + C_{UC,Conv} + C_{UC,DU}}{C_{UC,Enr}}. \tag{66}$$

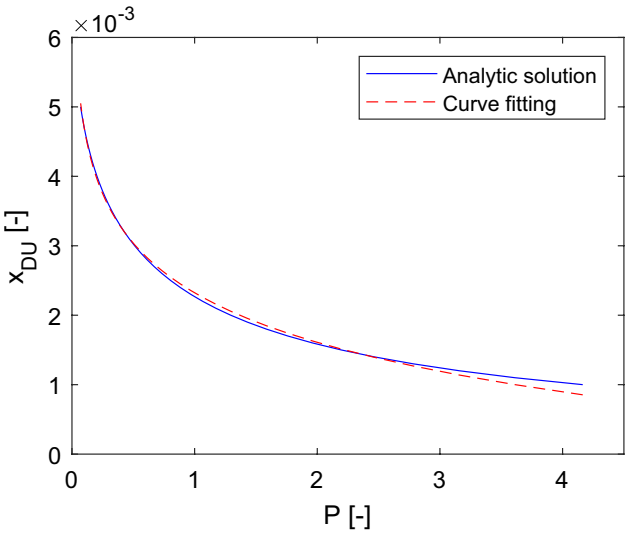


**Fig. 2** Relation curve between $P$ and optimal $x_{DU}$

And the relationship between $P$ and optimal $x_{DU}$ can be derived as follows:

$$P = X_{NU} - (2x_{NU} - 1) \times \ln\left(\frac{x_{DU}}{1 - x_{DU}}\right) - \frac{(2x_{DU} - 1) \times (x_{NU} - x_{DU})}{x_{DU} \times (1 - x_{DU})}. \quad (67)$$

As shown in Fig. 2, the optimal $x_{DU}$ is inversely proportional to $P$. When $P$ is small, indicative of a relatively high enrichment cost, the optimal $x_{DU}$ has a large value, making it more economical due to the reduction in enrichment work required. Conversely, when $P$ is large, the optimal $x_{DU}$ is smaller, which also results in economic benefits. An approximate solution for the optimal $x_{DU}$ can be derived by employing curve fitting with a simple logarithmic function of $P$, as follows:

$$x_{DU} = -0.00103 \times \ln(P) + 0.002323. \quad (68)$$

The calculation equations for the BE fuel cycle cost are as follows:

$$C^t_{FC,BE} = C^t_{SFcond} + C^t_{IS} + C^t_{SFdis} + C^t_{Pyro} + C^t_{TRUsto} + C^t_{RUdis} + C^t_{Wcond} + C^t_{Wdis} + C^t_{Decay}, \quad (69)$$

$$C^t_{SFcond} = \sum_i \left(M^t_{i,SFcond} \times C_{UC,SFcond}\right), \quad (70)$$

$$C^t_{IS} = \sum_i \left(M^t_{i,IS} \times C_{UC,IS}\right), \quad (71)$$

$$C^t_{SFdis} = \sum_i \left(M^t_{i,SFdis} \times C_{UC,SFdis}\right), \quad (72)$$

$$C^t_{Pyro} = \sum_i \left(M^t_{i,Pyro} \times C_{UC,Pyro}\right), \quad (73)$$

$$C^t_{TRUsto} = \sum_i \left(M^t_{i,TRU} \times C_{UC,TRUsto}\right), \quad (74)$$

$$C^t_{RUdis} = \sum_i \left(M^t_{i,RU} \times C_{UC,RUdis}\right), \quad (75)$$

$$C^t_{Wcond} = \sum_i \left(M^t_{i,HLWcond} \times C_{UC,HLWcond} + M^t_{i,LILWcond} \times C_{UC,LILWcond}\right), \quad (76)$$

$$C^t_{Wdis} = \sum_i \left(M^t_{i,HLWdis} \times C_{UC,HLWdis} + M^t_{i,LILWdis} \times C_{UC,LILWdis}\right), \quad (77)$$

$$C^t_{Decay} = \sum_i \left(M^t_{i,Decay} \times C_{UC,Decay}\right), \quad (78)$$

where $C^t_{SFcond}$, $C^t_{IS}$, $C^t_{SFdis}$, $C^t_{Pyro}$, $C^t_{TRUsto}$, $C^t_{RUdis}$, $C^t_{Wcond}$, $C^t_{Wdis}$, and $C^t_{Decay}$ denote the costs expended for the SF conditioning and packaging, interim storage, SF disposal, pyro-processing, TRU storage, RU storage and disposal, radioactive waste conditioning and packaging, radioactive waste disposal, and decaying storage at time $t$, respectively. And $C_{UC,SFcond}$, $C_{UC,IS}$, $C_{UC,SFdis}$, $C_{UC,Pyro}$, $C_{UC,TRUsto}$, $C_{UC,RUdis}$, $C_{UC,HLWcond}$, $C_{UC,LILWcond}$, $C_{UC,HLWdis}$, $C_{UC,LILWdis}$, and $C_{UC,Decay}$ represent the unit costs of the SF conditioning and packaging, interim storage, SF disposal, pyro-processing, TRU storage, RU storage and disposition, radioactive waste conditioning and packaging, radioactive waste disposal, and decaying storage, respectively.

## Mass Analysis

### Transition Scenario to Fuel Cycle System Options

For mass analysis, it is crucial to define a transition scenario that includes timelines for the deployment of facilities or services within the fuel cycle system, in accordance with the national plan. The Korean government's recent announcement of the "10th Basic Plan on Electricity Demand and Supply (2022–2036)" [23] highlighted the construction of six new reactors and the lifespan extension of 12 existing reactors until 2036. The completion of the Shin-Hanul Units 1 and 2 and Shin-Gori Units 5 and 6 is anticipated between 2022 and 2025. Additionally, the previously canceled construction of Shin-Hanul Units 3 and 4 will restart, with completion expected between 2032 and 2033. Given the absence of a clear post-2037 plan, it is assumed that the 12 reactors whose lifespans have

**Table 1** Reactor operation plan based on "10th Basic Plan on Electricity Demand and Supply (2022 ~ 2036)" with consistent lifespans

| Type | Unit name | Power capacity (MWe) | Operation start (yr) | Operation end (yr) | Amount of spent fuel in storage at the end of 2022 (ton) | Initial fuel loading (ton) | Annual fuel loading (ton) |
|---|---|---|---|---|---|---|---|
| PWR | Kori1 | 587 | 1978 | 2017 | 209 | 52 | 17 |
| | Kori2 | 650 | 1983 | 2043 | 322 | 52 | 17 |
| | Kori3 | 950 | 1984 | 2044 | 866 | 68 | 19 |
| | Kori4 | 950 | 1985 | 2045 | 847 | 68 | 19 |
| | Shin-Kori1 | 1000 | 2010 | 2070 | 379 | 76 | 20 |
| | Shin-Kori2 | 1000 | 2011 | 2071 | 405 | 76 | 20 |
| | Saewool1 | 1400 | 2016 | 2076 | 127 | 104 | 29 |
| | Saewool2 | 1400 | 2017 | 2077 | 86 | 104 | 29 |
| | Saewool3 | 1400 | 2024 | 2084 | 0 | 104 | 29 |
| | Saewool4 | 1400 | 2025 | 2085 | 0 | 104 | 29 |
| | Hanbit1 | 950 | 1985 | 2045 | 788 | 68 | 19 |
| | Hanbit2 | 950 | 1986 | 2046 | 668 | 68 | 19 |
| | Hanbit3 | 1000 | 1994 | 2054 | 420 | 76 | 20 |
| | Hanbit4 | 1000 | 1995 | 2055 | 384 | 76 | 20 |
| | Hanbit5 | 1000 | 2001 | 2061 | 366 | 76 | 20 |
| | Hanbit6 | 1000 | 2002 | 2062 | 395 | 76 | 20 |
| | Hanul1 | 950 | 1987 | 2047 | 398 | 68 | 19 |
| | Hanul2 | 950 | 1988 | 2048 | 379 | 68 | 19 |
| | Hanul3 | 1000 | 1997 | 2057 | 491 | 76 | 20 |
| | Hanul4 | 1000 | 1998 | 2058 | 498 | 76 | 20 |
| | Hanul5 | 1000 | 2003 | 2063 | 485 | 76 | 20 |
| | Hanul6 | 1000 | 2004 | 2064 | 518 | 76 | 20 |
| | Shin-Hanul1 | 1400 | 2022 | 2082 | 15 | 104 | 29 |
| | Shin-Hanul2 | 1400 | 2023 | 2083 | 0 | 104 | 29 |
| | Shin-Hanul3 | 1400 | 2032 | 2092 | 0 | 104 | 29 |
| | Shin-Hanul4 | 1400 | 2033 | 2093 | 0 | 104 | 29 |
| | Shin-Wolsung1 | 1000 | 2012 | 2072 | 201 | 76 | 20 |
| | Shin-Wolsung2 | 1000 | 2014 | 2074 | 140 | 76 | 20 |
| PHWR | Wolsung1 | 679 | 1982 | 2018 | 622 | 87 | 103 |
| | Wolsung2 | 700 | 1996 | 2036 | 736 | 87 | 103 |
| | Wolsung3 | 700 | 1997 | 2037 | 779 | 87 | 103 |
| | Wolsung4 | 700 | 1999 | 2039 | 779 | 87 | 103 |
| | Dry storage | – | – | – | 6,528 | – | – |

been extended to 2036 will be decommissioned simultaneously in 2037, despite their varying lifespans. However, for consistency and simplicity in planning, it is reasonable to assume a uniform operational lifespan for all: 60 years for PWRs and 50 years for PHWRs. The operational details of these reactors are summarized in Table 1, with data referenced from the "(1st) Basic Plan on HLW Management" [24]. For the purpose of this analysis, the conversion factor from assemblies to tons was taken as 0.43 ton/assembly for PWR fuel and 0.019 ton/assembly for PHWR fuel.

In 2021, following extensive public involvement and in line with the Radioactive Waste Management Act, the Korean government unveiled the "2nd Basic Plan on HLW Management" [25]. This comprehensive plan outlines a gradual approach to managing HLW, detailing the processes for selecting sites for management facilities based on social consensus and the plan for establishing and operating these facilities. According to the proposed timeline, securing a site is anticipated within 13 years, an interim storage facility within 20 years, and a final disposal facility within 37 years. Adhering to this plan, a transition scenario for the OT cycle can be formulated. Assuming site selection starting in 2024, the operation of the interim storage facility is expected to begin in 2045, and the final disposal facility is slated to start in 2062. Spent fuels in AR storage facilities can be transferred to the interim

**Table 2** Reactor design parameters and compositions of fresh fuel and spent fuel

| | | PWR | SFR | PHWR |
|---|---|---|---|---|
| Power capacity (MWe) | | 587 ~ 1,400 | 1,000 | 679 ~ 700 |
| Avg. burn-up (GWd/tU) | | 44* | 138 | 6* |
| Thermal efficiency (%) | | 34 | 39 | 34 |
| Capacity factor (%) | | 85 | 85 | 85 |
| Residence time (yr) | | 3.1* | 3.4 | 0.7* |
| Construction time (yr) | | 5 | 5 | 5 |
| Fresh fuel composition | | U-235 4.5% | TRU 38.87% | U-235 0.711% |
| Spent fuel composition (%) | U | 92.92 | 55.41 | 98.74 |
| | TRU | 1.36 | 30.40 | 0.41 |
| | FP | 5.72 | 14.19 | 0.85 |

* Averaged value

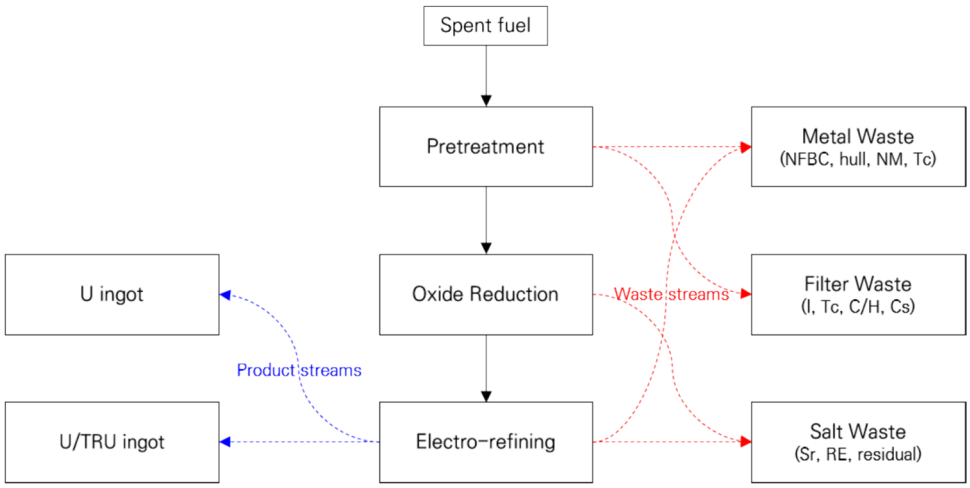


**Fig. 3** Simple process flow with waste and product streams of pyro-processing

storage facility after a cooling period of 10 years and to the final disposal facility after 40 years of cooling. The annual transport limit for spent fuel to both the interim storage and final disposal facilities is set at 1,000 tons. It is assumed that all spent fuels will be stored at the interim storage facility before their eventual disposal at the final disposal facility.

In alignment with the operational plan for the interim storage and final disposal facilities outlined in the transition scenario to the OT cycle, the transition to the pyro-SFR cycle necessitates additional operational plans for the SFR, pyro-processing facilities, and associated infrastructures. Given the current advancement level of pyro-processing technology, it is assumed that the pyro-processing facility will start its operation by 2050, 5 years subsequent to the commencement of the interim storage facility. Therefore, PWR spent fuels will be stored at an interim storage facility prior to undergoing pyro-processing. The HLW produced by the pyro-processing facility will be stored at the interim storage facility before being transferred to the final disposal facility. Radioactive wastes emitting high levels of heat will be kept in long-term decay storage, eventually being moved to disposal sites designated for LILW. To avert the accumulation of plutonium, it is anticipated that both the SFR fuel fabrication facility and the SFRs will commence operations concurrently with the initiation of the pyro-processing facility. The operational plan for the SFRs is derived through mass analysis, which assesses the amount of TRU stocks and SFR spent fuels generated.

**Table 3** Volume and element mass of wastes generated from pyro-processing

| Class | PWR spent fuel | | SFR spent fuel | |
|---|---|---|---|---|
| | Volume | Element mass | Volume | Element mass |
| HLW | – | 13.3 kgFP/tHM | – | 62.4 kgFP/tHM |
| LILW | 2.3 $m^3$/tHM | – | 2.6 $m^3$/tHM | – |
| Cs/Sr | – | 5.3 kgCsSr/tHM | – | 16.7 kgCsSr/tHM |

## Input Parameters

Table 2 summarizes the reactor design parameters and fuel composition details. The average burn-up and residence time are derivable from Eqs. (7), (8), (19), and (20), utilizing the fuel loading information provided in Table 1, alongside the presupposed figures for thermal efficiency and capacity factor. For the SFR, the design parameters are informed by the conceptual design developed at the KAERI. To ascertain the mass flow for the BE cycle, the compositions of the spent fuels were determined through depletion and decay calculations.

Mass-flow analysis for pyro-processing was conducted to determine the quantity of waste generated from pyro-processing activities, which then served as input parameters for the economic evaluation. The flow diagram for pyro-processing of PWR spent fuel delineates three primary processes: pretreatment, oxide reduction, and electrorefining, as depicted in Fig. 3. In contrast, pyro-processing of SFR spent fuel does not include the oxide reduction step, because SFR spent fuel, being metallic, can be directly introduced into the electrorefining process. From these main processes, three types of waste are produced: metal, filter, and salt wastes. Concurrently, two types of products are generated: one containing U and the other comprising U/TRU ingots.

The volume and elemental mass for each type of waste stream were determined through mass-flow analysis, as illustrated in Table 3. In accordance with Korea's classification of radioactive waste, HLW is characterized by radioactivity exceeding 4,000 Bq/g for alpha-emitting nuclides with a half-life longer than 20 years, and a heat generation rate surpassing 2 kW/m$^3$. The RE salt waste, containing substantial amounts of FPs and a minor quantity of TRUs, can be classified as HLW, despite not meeting the heat generation rate criterion of 2 kW/m$^3$. Metal and filter wastes, along with secondary wastes such as consumables and devices generated during operations, are categorized as LILW. Filter waste, which includes cesium (Cs), and salt waste, containing strontium (Sr), are classified as Cs/Sr wastes and allocated to long-term decay storage.

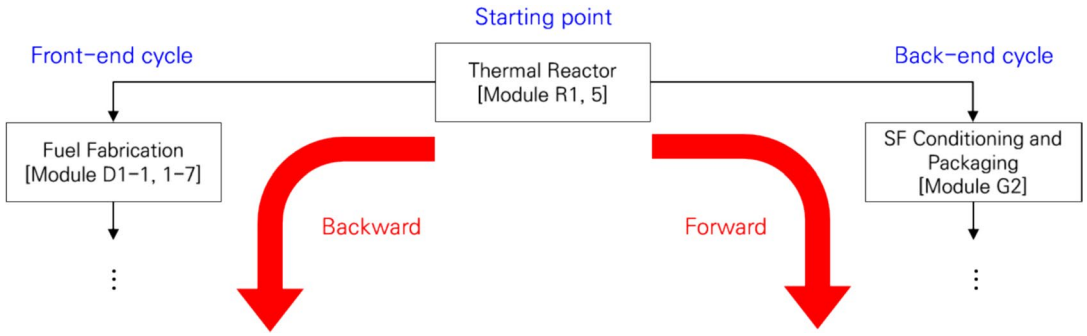


**Fig. 4** Calculation of mass flows for all modules in the fuel cycle system

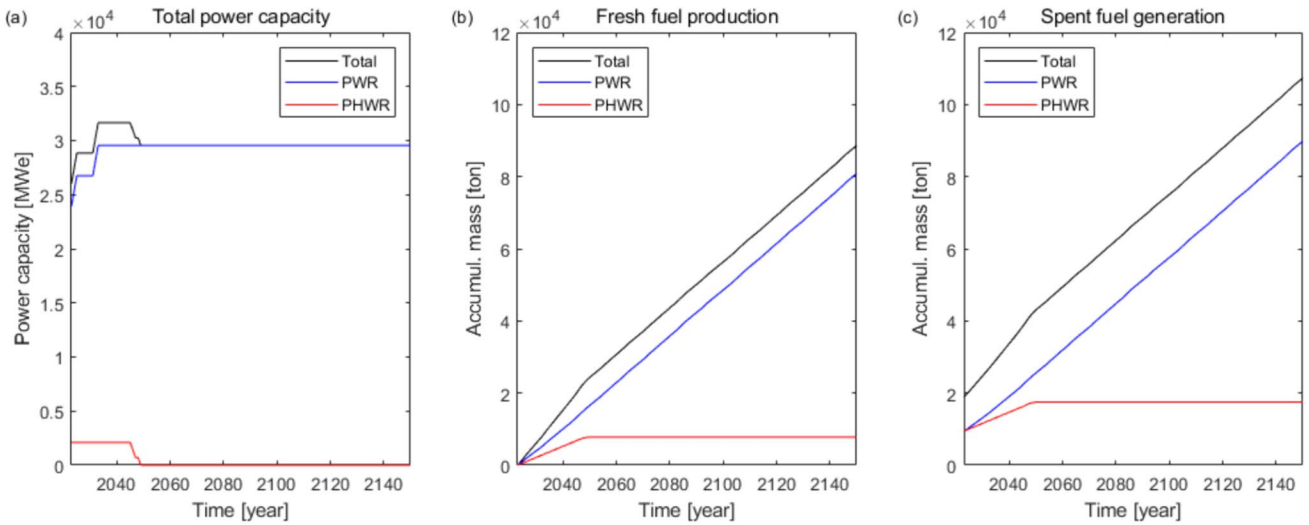


**Fig. 5** Future prediction of total power capacity (**a**), fresh fuel production (**b**), and spent fuel generation (**c**)

Given that the amount of LILW generated from other fuel cycle facilities is relatively small [17], conducting a mass-flow analysis to ascertain the volume of LILW for these facilities is deemed unnecessary for the purposes of economic evaluation.

## Mass Analysis Result

The mass flows for each module within the fuel cycle system are derived by solving the mass-flow model, a system of algebraic equations, as depicted in Fig. 4. The initial step involves calculating the amount of fresh fuel loaded into the reactors and the amount of spent fuel generated from the operation of both PWRs and PHWRs. After determining the amounts of fresh and spent fuels, the mass flows for the FE cycle modules are obtained in reverse order, while those for the BE cycle modules are determined in a forward sequence by solving the respective equations. This calculation process is iterated at every time step from the beginning until the end of the specified period.

A scenario for the future total power capacity, fresh fuel production, and spent fuel generation of PWRs and PHWRs has been made, as illustrated in Fig. 5. In line with the national plan (as detailed in Table 1), the total power capacity is projected to reach 31.65 GWe by 2036. For the period from 2037 onwards, it is assumed that the total power capacity of PHWRs will decline to 0 GWe by 2049 as planned, while the total power capacity of PWRs in 2036 will be maintained by replacing old reactors to new ones of the same power capacity. To support this power capacity, it is necessary to produce 88,000 tons of fresh fuel, comprising 80,200 tons for PWRs and 7,800 tons for PHWRs until 2150, which is the final year of the evaluation period. The total anticipated generation of spent fuel until 2150 is 107,300 tons, with 89,800 tons originating from PWRs and 17,500 tons from PHWRs, which includes the current amount of spent fuels stored in AR storage facilities (Table 1).

In the process of calculating mass flows for the FE and BE cycle modules within the pyro-SFR cycle, a critical step involves formulating an operational plan for the SFRs that aims at completely utilizing all TRUs present in the future stockpile of PWR spent fuels. Reflecting on the current pace of research and development in Korea, it was assumed that a commercial SFR with a capacity of 1 GWe could be operational after 2050, with multiple SFRs being commissioned gradually by replacing PWRs. In this simulation study, the inventory of TRU in the SFR fuel fabrication facility and the amount of SFR spent fuel stored in the interim storage were analyzed by adjusting the number of operational SFRs over an extended period, as illustrated in Fig. 6. It is critical that the TRU stock does not fall into negative values, which would imply a necessity to import TRUs. Operating 11 SFRs is deemed appropriate as neither result in deficit of the TRU stock nor accumulates a large amount of SFR spent fuel.

After setting the operation plan for all reactors, the mass flows for the FE and BE cycle modules included in both the OT and pyro-SFR cycle options were calculated, as depicted in Fig. 7. The accumulative mass flows for the FE cycle modules of the pyro-SFR cycle in 2150 are lower than those of the OT cycle due to reduced PWR operation (Fig. 7a–d). The mass flow of the NU mining module serves as an indicator for quantitatively evaluating resource requirement (Fig. 7a). Thus, in terms of resource requirement, the pyro-SFR cycle presents a more advantageous option compared to the OT cycle. For the BE cycle modules, the accumulative mass flows of the pyro-SFR cycle in 2150 are much lower than those of the OT cycle (Fig. 7e, f). When examining the mass flow of the interim storage module (Fig. 7e), the mass

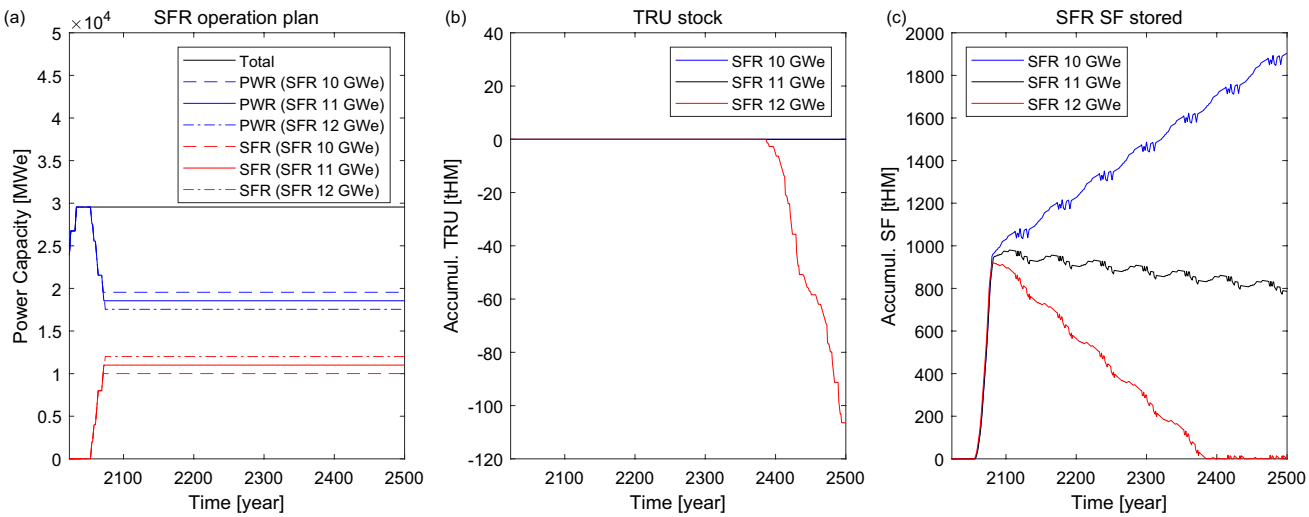


**Fig. 6** SFR operation planning (**a**), by checking TRU stocks in the fuel fabrication facility (**b**), and SFR spent fuels in the interim storage (**c**)

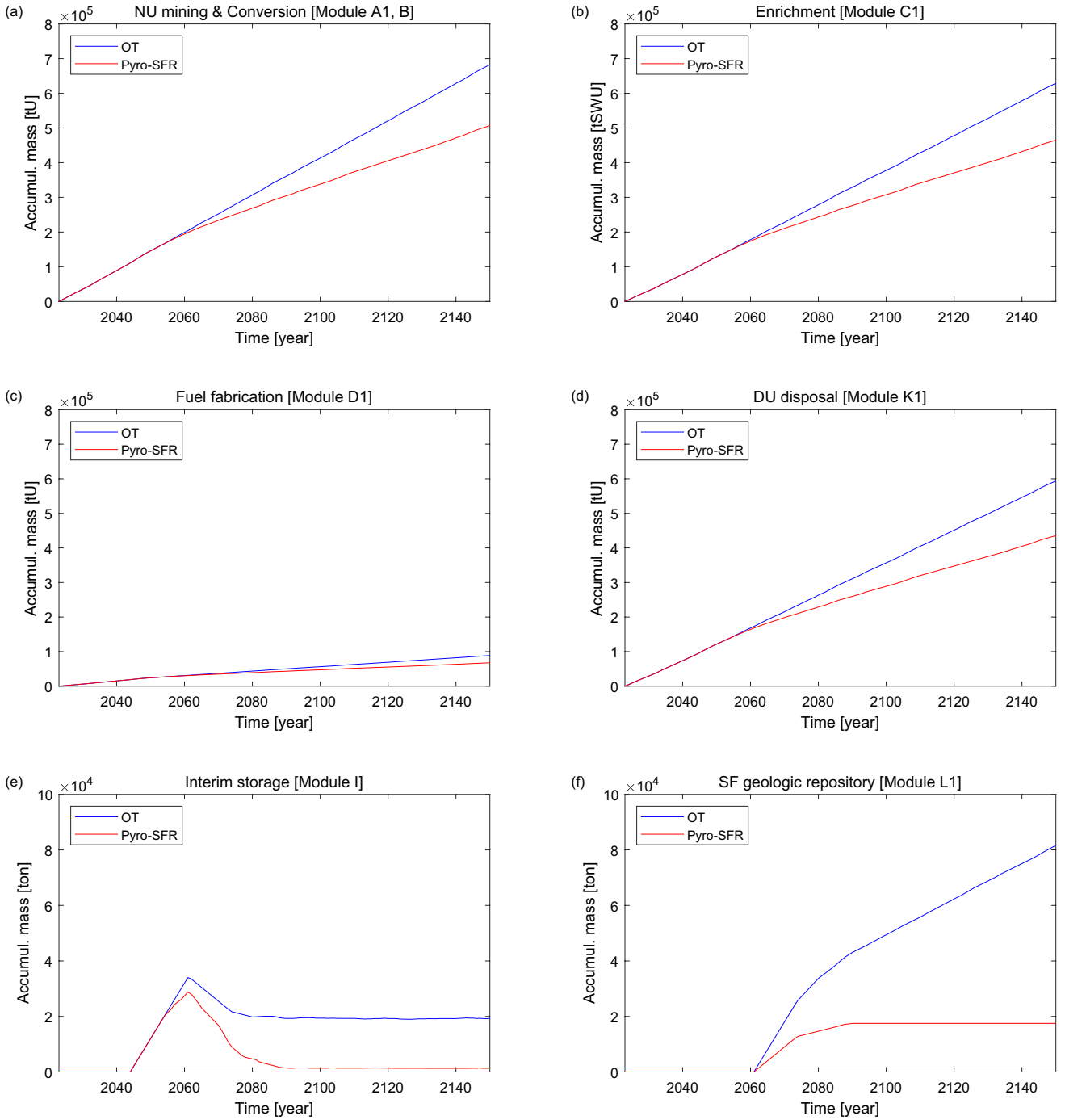


**Fig. 7** Mass flows of the FE and BE fuel cycle modules: **a** NU mining, **b** enrichment, **c** fuel fabrication, **d** DU disposal, **e** interim storage, and **f** SF geologic repository

flow of the pyro-SFR cycle is significantly reduced due to the removal of PWR spent fuels from the interim storage for pyro-processing. As a result, the storage capacity needed for the interim storage facility during the static period is approximately 1,500 tons, which is less than one-tenth of that required for the OT cycle. Regarding the geological

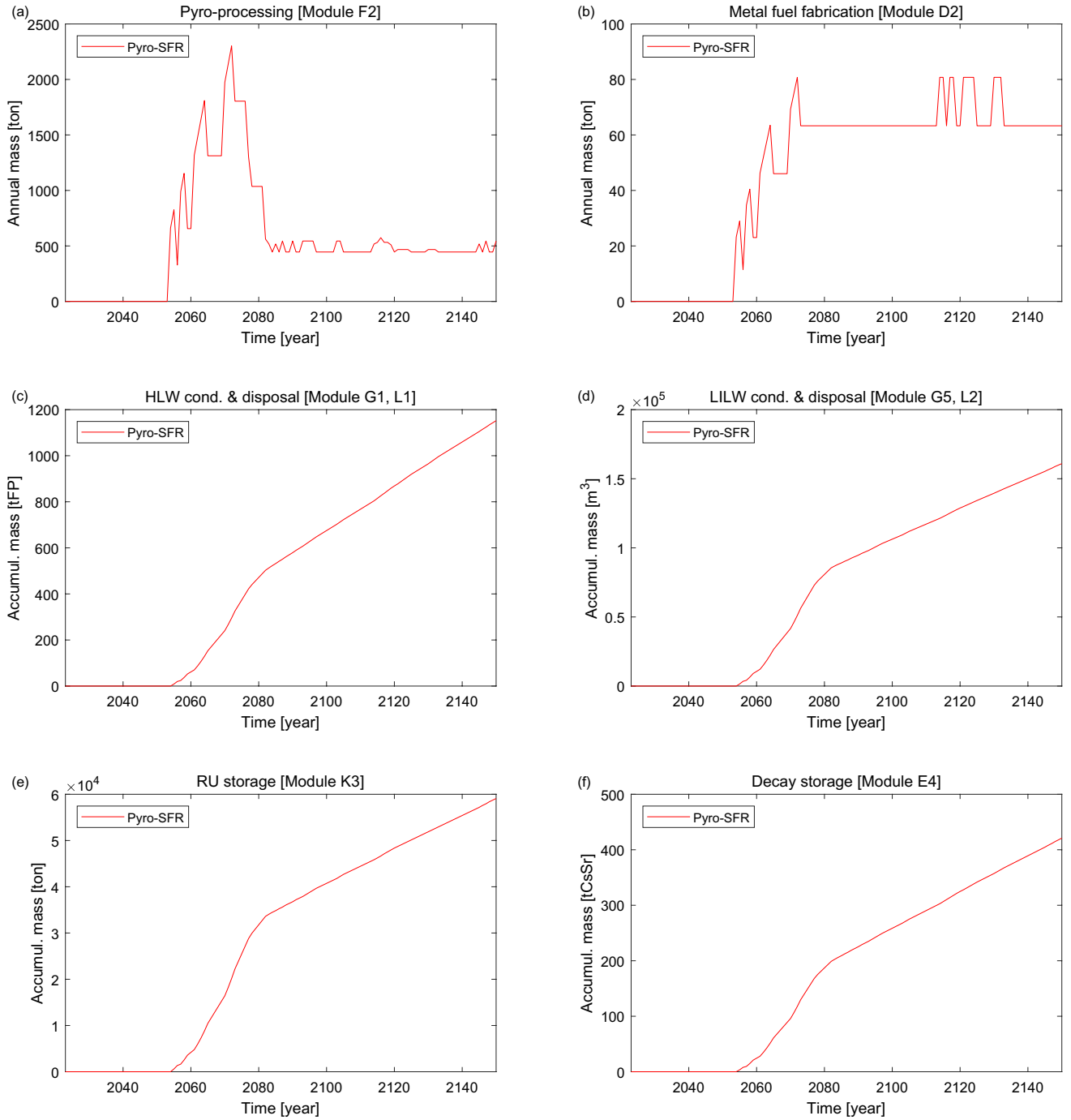


**Fig. 8** Mass flows of the BE fuel cycle modules in the pyro-SFR cycle option: **a** pyro-processing, **b** metal fuel fabrication, **c** HLW conditioning and disposal, **d** LILW conditioning and disposal, **e** RU storage, and **f** decay storage

repository (Fig. 7f), the accumulative mass flow of the pyro-SFR cycle in 2150 is 17,500 tons originating only from PHWRs, while that of the OT cycle is 81,000 tons originating from both PWRs and PHWRs.

Figure 8 shows the mass flows for additional BE cycle modules of the pyro-SFR cycle option. Spent fuels and fresh fuels are processed and produced solely in amounts needed for SFR operation in the pyro-processing and metal fuel fabrication modules, respectively, ensuring that TRUs do not accumulate in recycled product storage (Fig. 8a, b). The accumulative quantities of spent fuels (Fig. 7f) and HLWs (Fig. 8c) serve as a quantitative indicator of HLW generation. Given that the amount of HLW generated from the pyro-SFR cycle is less than that from the OT cycle, the

**Table 4** Unit costs for the modules of reactors and fuel cycle facilities from Advanced Fuel Cycle Cost Basis Report (AFC-CBR) 2017 [21]

| | Module | Units | Low | Mode | High | Mean | PDF |
|---|---|---|---|---|---|---|---|
| PWR (overnight capital) | R1 | $/kWe | 2500 | 4400 | 6300 | 4400 | Triangular |
| PWR (O&M, fixed component) | R1 | $/kWe-yr | 60 | 73 | 87 | 73 | Triangular |
| PWR (O&M, variable component) | R1 | $/kWh | 0.0008 | 0.0018 | 0.0027 | 0.0018 | Triangular |
| SFR (overnight capital) | R2 | $/kWe | 2400 | 4100 | 7600 | 4700 | Triangular |
| SFR (O&M, fixed component) | R2 | $/kWe-yr | 65 | 76 | 92 | 78 | Triangular |
| SFR (O&M, variable component) | R2 | $/kWh | 0.0011 | 0.0022 | 0.0029 | 0.0021 | Triangular |
| PHWR (overnight capital) | R5 | $/kWe | 2400 | 4200 | 6100 | 4230 | Triangular |
| PHWR (O&M, fixed component) | R5 | $/kWe-yr | 60 | 72 | 87 | 73 | Triangular |
| PHWR (O&M, variable component) | R5 | $/kWh | 0.0008 | 0.002 | 0.0027 | 0.0018 | Triangular |
| NU mining and milling | A1 | $/kgU | 34 | 86 | 296 | 139 | Triangular |
| Conversion | B | $/kgU | 6.5 | 13 | 19 | 13 | Uniform |
| Enrichment | C1 | $/SWU | 97 | 125 | 154 | 125 | Uniform |
| PWR fuel fabrication | D1-1 | $/kgHM | 230 | 400 | 575 | 402 | Triangular |
| PHWR fuel fabrication | D1-7 | $/kgHM | 125 | 218 | 327 | 223 | Triangular |
| Metal fuel fabrication | D2 | $/kgHM | 1000 | 1400 | 1800 | 1400 | Triangular |
| Recycled product storage | E3 | $/kgHM | 712 | 950 | 1300 | 987 | Triangular |
| Managed decay storage | E4 | $/kgCs-Sr | 11,400 | 25,650 | 39,900 | 25,650 | Triangular |
| Echem separation | F2 | $/kgHM | 1000 | 1200 | 1400 | 1200 | Triangular |
| HLW conditioning and packaging | G1 | $/kgFP | 13,700 | 17,214 | 20,660 | 17,191 | Triangular |
| SF conditioning and packaging | G2 | $/kgHM | 67.5 | 135 | 175 | 126 | Triangular |
| LLW-GTCC conditioning and packaging | G4 | $/m$^3$ | 10,800 | 12,770 | 17,100 | 13,560 | Triangular |
| Consolidated interim storage | I | $/kgHM | 223 | 501 | 644 | 456 | Triangular |
| DU storage and disposition | K1 | $/kgHM | 8.8 | 20.6 | 54.5 | 28 | Triangular |
| RU storage and disposition | K3 | $/kgU | 81.8 | 98.1 | 164 | 115 | Triangular |
| HLW deep geologic repository | L1 | $/kgHM | 1500 | 6000 | 7500 | 5000 | Triangular |
| SF deep geologic repository | L1 | $/kgHM | 289 | 600 | 873 | 587 | Triangular |
| GTCC intermediate depth disposal | L2 | $/m$^3$ | 2300 | 3800 | 5320 | 3807 | Uniform |

pyro-SFR cycle could be considered as a preferable choice. The final amount of LILWs (Fig. 8d) also offers a basis for comparison between the two options. Although LILWs exhibit lower heat and radioactivity levels compared to HLWs, the pyro-SFR cycle contributes to an increased generation of LILWs; hence, from this perspective, the OT cycle might be considered more favorable. Notably, since approximately 93% of PWR spent fuel comprises U, a considerable amount of RUs is separated during pyro-processing and remains largely unused as SFR fresh fuel (Fig. 8e). RU, characterized by substantially lower heat and radioactivity levels than HLW, presents minimal storage and disposal challenges. In this analysis, RU is envisaged as a potential resource, either for import or for future fuel production. Additionally, radioactive wastes including high heat-emitting radionuclides, generated during pyro-processing, can be disposed of as LILW after decay storage due to their short half-life (Fig. 8f).

## Economic Evaluation

### Unit Cost Preparation

In this paper, the unit cost data for economic evaluation were sourced from the INL Advanced Fuel Cycle Cost Basis Report (AFC-CBR) 2017 edition [21], recognized for its comprehensive compilation of unit costs across various fuel cycle options. This database has undergone several revisions from 2004 to 2017, contributed by multiple US national laboratories under the Department of Energy-Nuclear Energy (DOE-NE), ensuring its accuracy and reliability. The unit costs relevant to the modules outlined in the system definition (Fig. 1) were directly extracted from the AFC-CBR 2017 and are detailed in Table 4. Table 4 provides the overnight capital and O&M cost for PWR, SFR, and PHWR alongside the costs associated with facilities involved in the FE and BE fuel cycles. Given that the AFC-CBR 2017 lists nominal unit costs in 2017, an adjustment to 2023—the base year for this economic evaluation—is required. This adjustment involves applying the US escalation factor, which

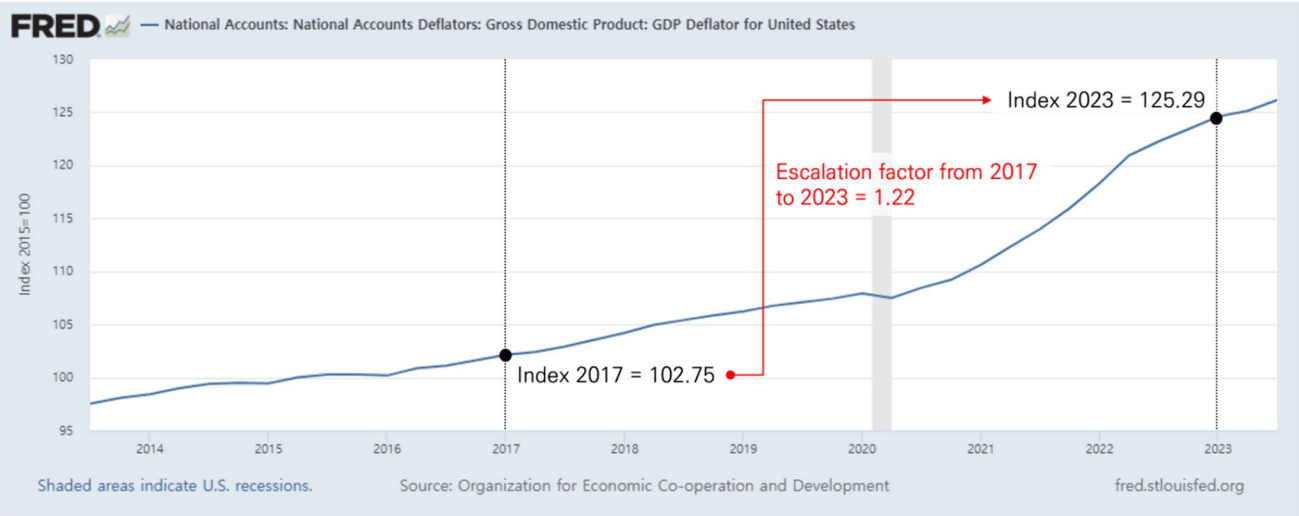


**Fig. 9** US escalation factor based on the FRED's US GDP deflator data [26]

accounts for inflation and economic growth since 2017. The escalation factor is determined using the ratio of the US Gross Domestic Product (GDP) deflator data, as provided by the Federal Reserve Economic Data (FRED) [26], depicted in Fig. 9.

The AFC-CBR provides mode and mean values for point value estimation reflecting the anticipated most likely cost value, and boundary values (low and high values) and a probability distribution type for sensitivity and uncertainty analysis. Due to the scarcity of cost information for each module, all probability distributions are straightforwardly defined as triangular or uniform. Triangular distributions were predominantly applied, except for modules B and C1, where historically wide variations in market prices have been observed, and for module L2 having several alternative technologies.

In this study, an economic evaluation was carried out by defining the size of the nuclear power system in Korea through mass analysis, which took into account possible transition scenarios. However, the mass flows identified for the Korean nuclear system differed from the capacities of the reference facilities utilized to derive the unit cost estimates in the AFC-CBR. When the mass flow of a particular module in the Korean nuclear system exceeds the capacity of the reference facility used for determining the unit cost in the AFC-CBR for the same module, the unit cost is adjusted downwards to reflect economies of scale. Conversely, if the mass flow in the Korean nuclear system is smaller than that of the reference, the unit cost from the AFC-CBR is increased to account for the lack of economies of scale. The formula to adjust unit costs based on economies of scale is specified as follows [21]:

$$\frac{C_{j,scaled}}{C_j} = \left(\frac{S_{j,scaled}}{S_j}\right)^{\alpha_j}, 0 \le \alpha_j \le 1, \tag{79}$$

where $C_{j,scaled}$ and $C_j$ denote the scaled and reference costs for module $j$, and $S_{j,scaled}$ and $S_j$ represent the capacity sizes of facilities for the scaled and reference costs for module $j$. $\alpha_j$ denotes the scaling factor for module $j$. From Eq. (79), an equation for the economies of scale in terms of the unit cost can be derived as follows:

$$C_{UC,j,scaled} = C_{UC,j} \times \left(\frac{S_j}{S_{j,scaled}}\right)^{1-\alpha_j}, 0 \le \alpha_j \le 1, \tag{80}$$

**Table 5** The capacity size and scaling factor of reference facility for the unit cost in Advanced Fuel Cycle Cost Basis Report (AFC-CBR) 2017 [21]

| Fuel cycle module | Reference facility | Scaling factor | Capacity size |
|---|---|---|---|
| DU disposition | DU disposition | 0.6 | 6,630 ton/y |
| Pyro-processing | Pyro-processing | 0.7 | 70 ton/y |
| Metal fuel fabrication | | | |
| RU disposition | | | |
| HLW conditioning and packaging | Pyro-processing | 0.6 | 300 ton/y |
| Recycled product storage | Recycled product storage | 0.41 | 50 ton (TRU)/y |

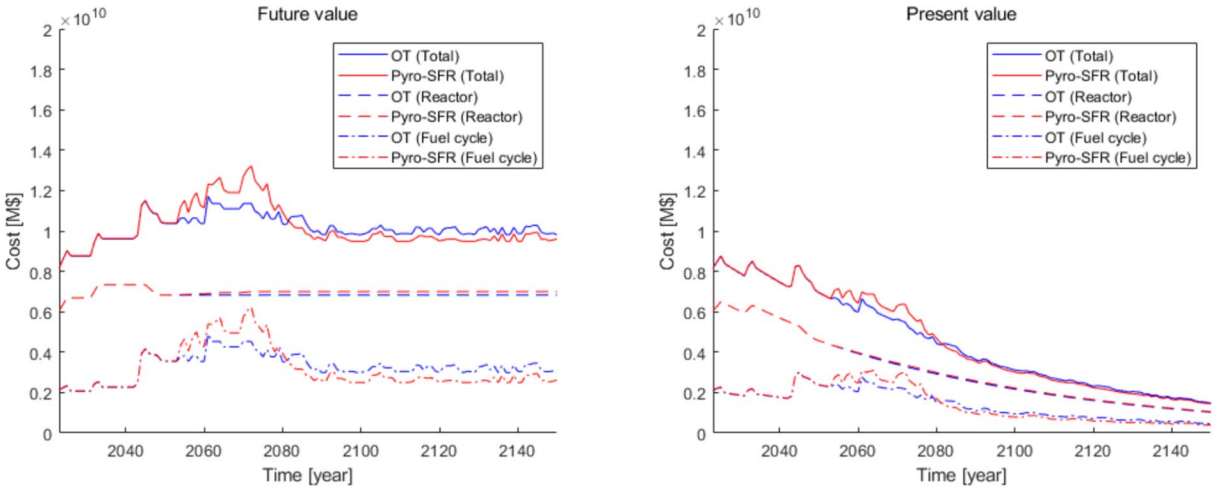


**Fig. 10** Comparison of future and present values over time for OT and pyro-SFR cycles

**Table 6** Cost breakdown of the total cost and LCOE for OT and pyro-SFR cycles

| | Future value [B$] | | Present value [B$] | | LCOE [mills/kWh] | |
|---|---|---|---|---|---|---|
| | OT | Pyro-SFR | OT | Pyro-SFR | OT | Pyro-SFR |
| Reactor capital | 539 | 548.4 | 243.5 | 246.4 | 19.05 | 19.28 |
| Reactor O&M | 340.1 | 345.2 | 153.5 | 155.1 | 12.01 | 12.14 |
| FE fuel cycle | 289.4 | 222 | 130.2 | 109.3 | 10.19 | 8.55 |
| BE fuel cycle | 130.9 | 185.8 | 53.6 | 77.8 | 4.2 | 6.09 |
| Total | 1,299.3 | 1,301.4 | 580.8 | 588.6 | 45.45 | 46.06 |
| Total electricity generation [TWh] | 28,315 | 28,315 | 12,779 | 12,779 | – | – |

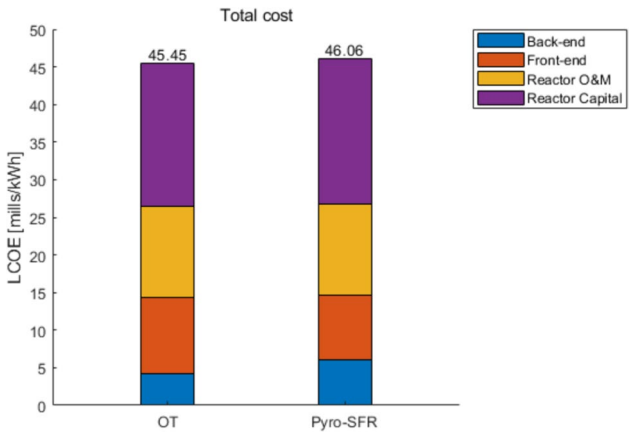


**Fig. 11** Comparison of LCOEs of total costs for OT and pyro-SFR cycles

$$S_{j,scaled} = M_{j,avg} = \frac{\sum_{t_{j,start}}^{t_{j,end}} M_j^t}{t_{j,end} - t_{j,start}}, \tag{81}$$

where $C_{UC,j,scaled}$ denotes scaled unit cost for module $j$. $M_{j,avg}$ represents the averaged mass flow of $M_j^t$ from the start, $t_{j,start}$ to the end, $t_{j,end}$ of operation for module $j$. The AFC-CBR suggests precise values of the capacity sizes and scaling factors of reference facilities for certain modules, as shown in Table 5 [21]. Specifically, the scaling factors in Table 5 were derived by fitting available cost data from various capacity sizes to Eq. (79).

AFC-CBR does not provide capacity sizes or scaling factors for all modules. For most FE fuel cycle modules with mature technologies, scale-up considerations are irrelevant, since unit costs are estimated based on prevailing market prices. Therefore, the scaling factors for these modules were assumed to be 1. Similarly, for BE fuel cycle modules featuring multiple alternative future technologies yet to be implemented, scale-up is not feasible. Hence, the scaling factor for such modules was assumed to be 1.

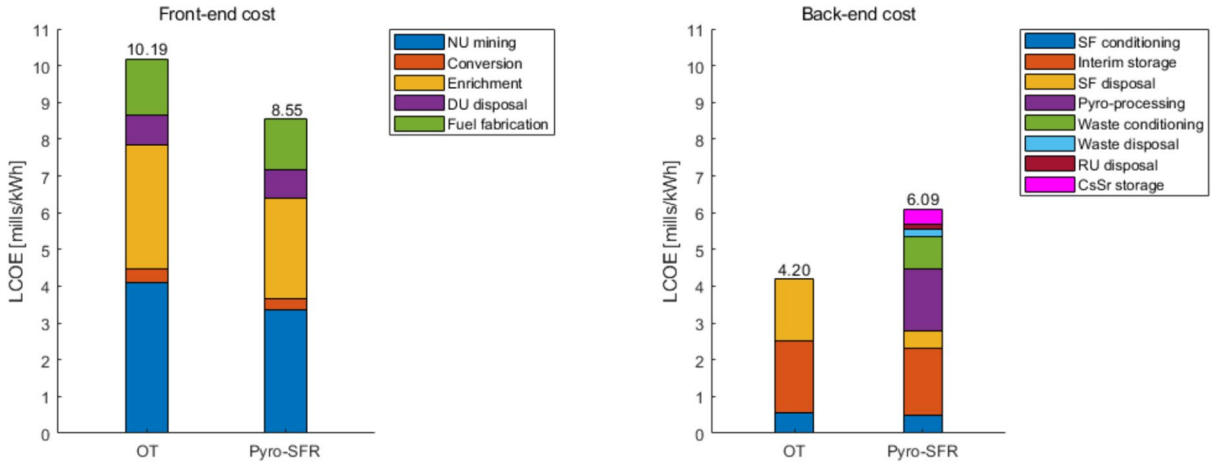


**Fig. 12** Comparison of LCOEs of fuel cycle costs for OT and pyro-SFR cycles

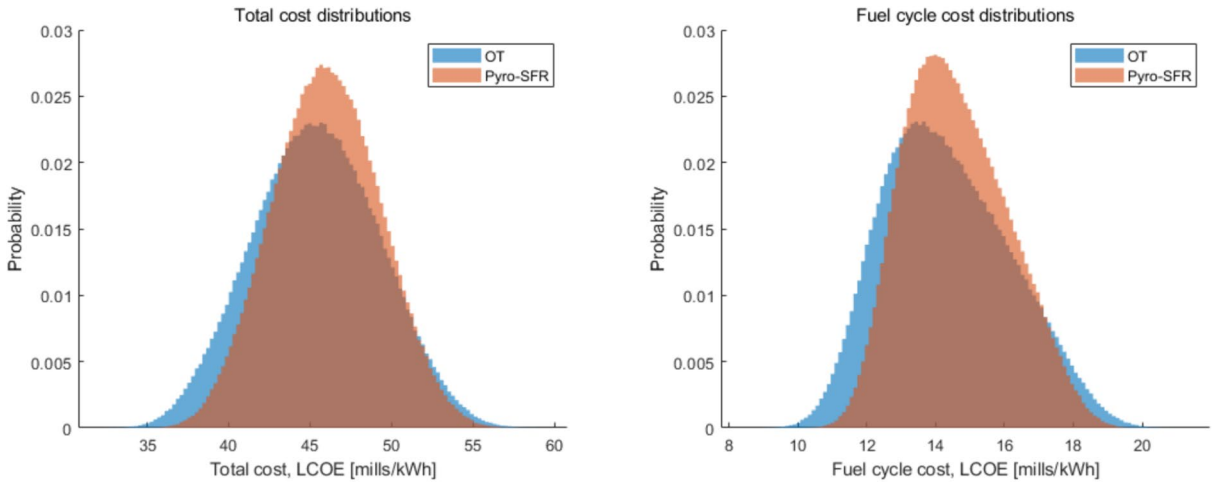


**Fig. 13** Cost distributions of the total and fuel cycle costs for OT and pyro-SFR cycles

## Economic Evaluation Result

By applying the unit costs to the mass analysis results for the OT and pyro-SFR cycle transition scenarios in Sect. 3.3, the future and present values of the total costs, including the reactor and fuel cycle costs, were obtained over time, as depicted in Fig. 10. By comparing the future and present values, it becomes apparent that the later the cost is expended, the greater the discount effect. This discount effect may vary significantly depending on the discount rate. For this calculation, a 1.5% real discount rate (equivalent to the interest rate) was employed based on the notice of the Korean government [27].

Table 6 presents the future and present values at all times. The future values of the reactor and BE fuel cycle costs for the pyro-SFR cycle surpass those for the OT cycle due to the additional operation of the SFR and related facilities in the BE fuel cycle. However, as these facilities were introduced relatively later (Figs. 6, 8), the differences in present values diminish due to the discount effect.

**Table 7** Statistical values of the cost distribution for OT and pyro-SFR cycles

| | Total cost | | Fuel cycle cost | |
|---|---|---|---|---|
| | Mean | STD | Mean | STD |
| OT [mills/kWh] | 45.40 | 3.85 | 14.34 | 1.84 |
| Pyro-SFR [mills/kWh] | 46.02 | 3.26 | 14.60 | 1.50 |

Dividing the present values of the costs by the present value of the total electricity generation yields the LCOEs, as depicted in Fig. 11 and Table 6. The LCOE of the total cost of the pyro-SFR cycle slightly exceeded that of the OT cycle. Notably, reactor capital and O&M costs for both

options were comparable, constituting more than 68% of the total costs. However, in the pyro-SFR cycle, additional expenditure on the BE fuel cycle surpassed saving on the FE fuel cycle. This result is not significantly different from the previous cost studies [14, 18, 19], which have estimated that the pyro-SFR cycle cost is 3 ~ 4% higher than the OT cycle cost. However, this study shows a reduced difference as economies of scale are reflected in the unit costs of pyro-processing and related modules (Table 5). Since the capacity size of the reference facility for unit cost estimation in AFC-CBR 2017 [21] is smaller than the amount processed in the Korean scenario, the economies of scale favor the pyro-SFR cycle, resulting in a reduced cost gap between the two cycles compared to previous studies.

Figure 12 compares the LCOEs of the FE and BE fuel cycle costs for both options. When comparing the FE cycle costs, the ratio of each cost is nearly equivalent for both options, but the absolute value of each cost for the pyro-SFR cycle diminishes due to the reduced PWR operation. Concerning the BE cycle cost of the pyro-SFR cycle, while the SF disposal cost, which is predominant in the OT cycle, decreases, other costs such as those associated with pyro-processing and waste conditioning are introduced.

The unit cost can vary between different technologies for the same module, as well as between different countries for the same technology. In addition, technologies that are still in development, such as pyro-processing and SFR, pose challenges in accurately predicting the unit cost of commercial-scale facilities. In essence, uncertainty

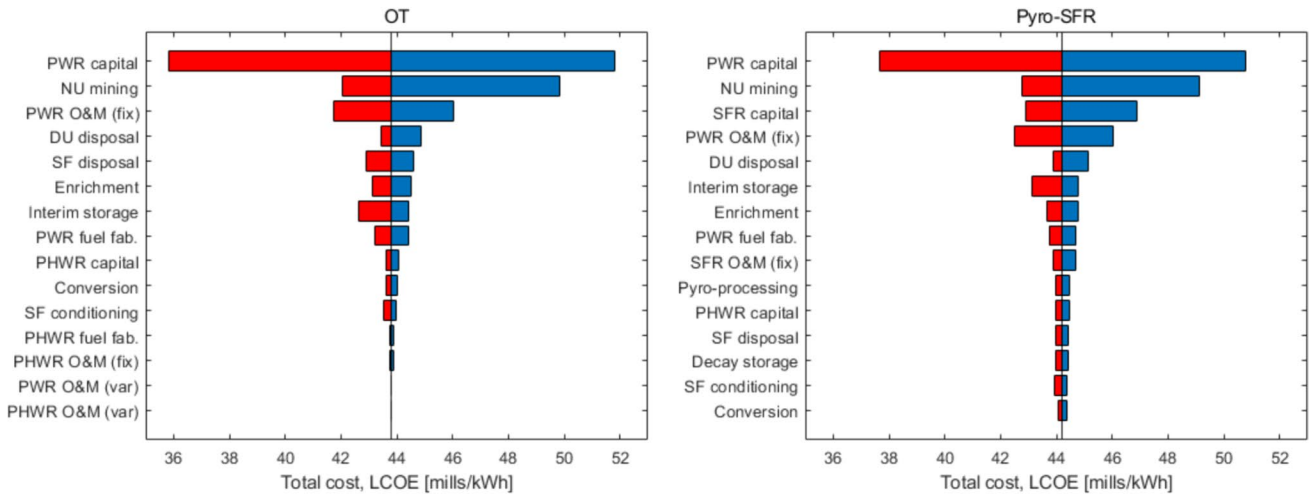


**Fig. 14** Tornado diagram of the total costs for OT and pyro-SFR cycles

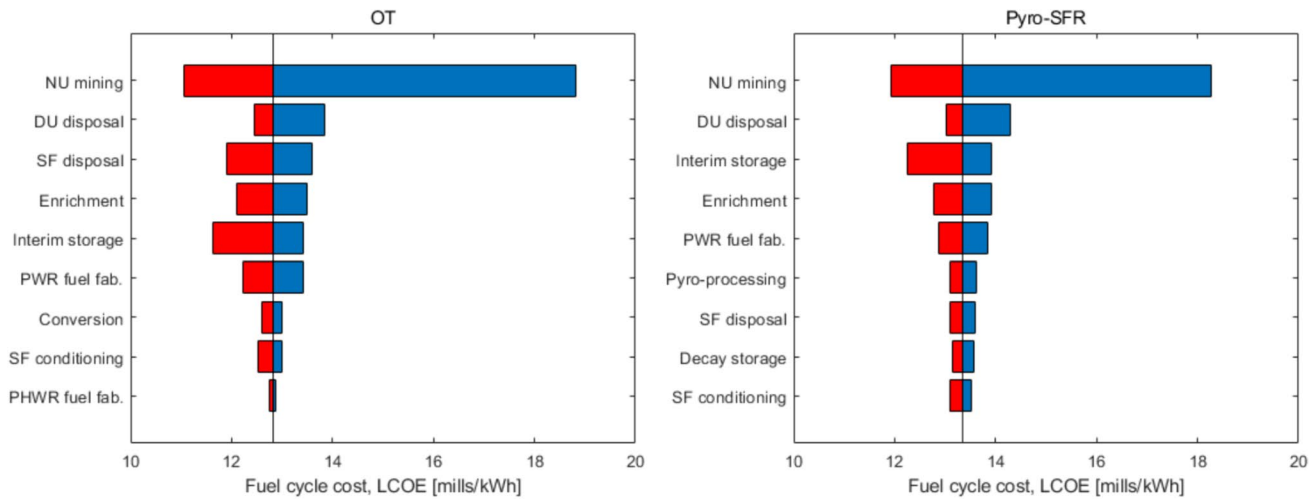


**Fig. 15** Tornado diagram of the fuel cycle costs for OT and pyro-SFR cycles

surrounds all unit costs and should be factored into an economic evaluation. As part of the uncertainty analysis, a Monte Carlo simulation using 1,000,000 random samples was conducted to derive the cost distributions for both options, as depicted in Fig. 13. The values on the y-axis represent the relative probabilities of cost occurrence. The relative heights of the distributions indicate the level of uncertainty. A narrower and taller cost distribution signifies lower cost uncertainty. The statistical values of the cost distributions are listed in Table 7.

Figure 13 illustrates that the pyro-SFR cycle exhibits less cost uncertainty for both total and fuel cycle costs. The largest portion of the total cost distribution pertains to reactor capital. In the case of the pyro-SFR cycle, the distribution is shaped by two large triangular distributions: one for PWR capital and another for SFR capital. When these distributions are convoluted in a certain proportion, they form a bell-shaped distribution that is narrower and taller than the triangular distribution alone, a phenomenon attributed to the central limit theorem [28]. Conversely, for the OT cycle, the total cost distribution is primarily determined by a single large triangular distribution representing PWR capital. The narrower distribution of fuel cycle costs for the pyro-SFR cycle is attributed to the reduced impact of high uncertainty in the unit cost of NU mining compared to the OT cycle. Among the unit costs listed in Table 4, NU mining exhibits the widest range. And as depicted in Fig. 12, the portion of NU mining cost in the FE cycle cost for the pyro-SFR cycle is smaller than that for the OT cycle.

A sensitivity analysis was conducted by varying the unit cost of individual modules from low to high values and observing the resulting changes in cost. Due to the relatively

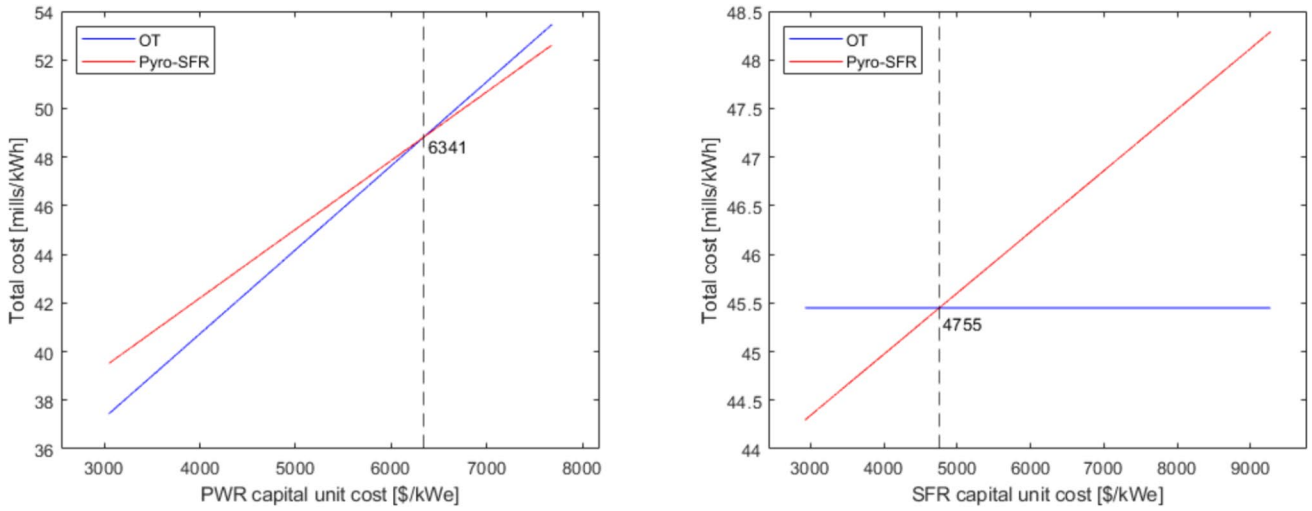


**Fig. 16** Break-even point analysis for the unit costs of PWR capital and SFR capital

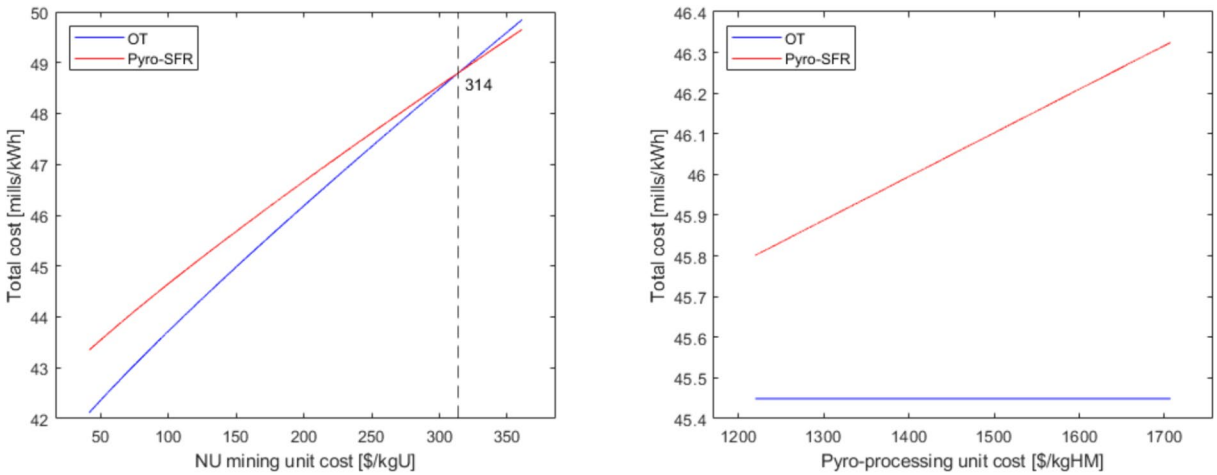


**Fig. 17** Break-even point analysis for the unit costs of NU mining and pyro-processing

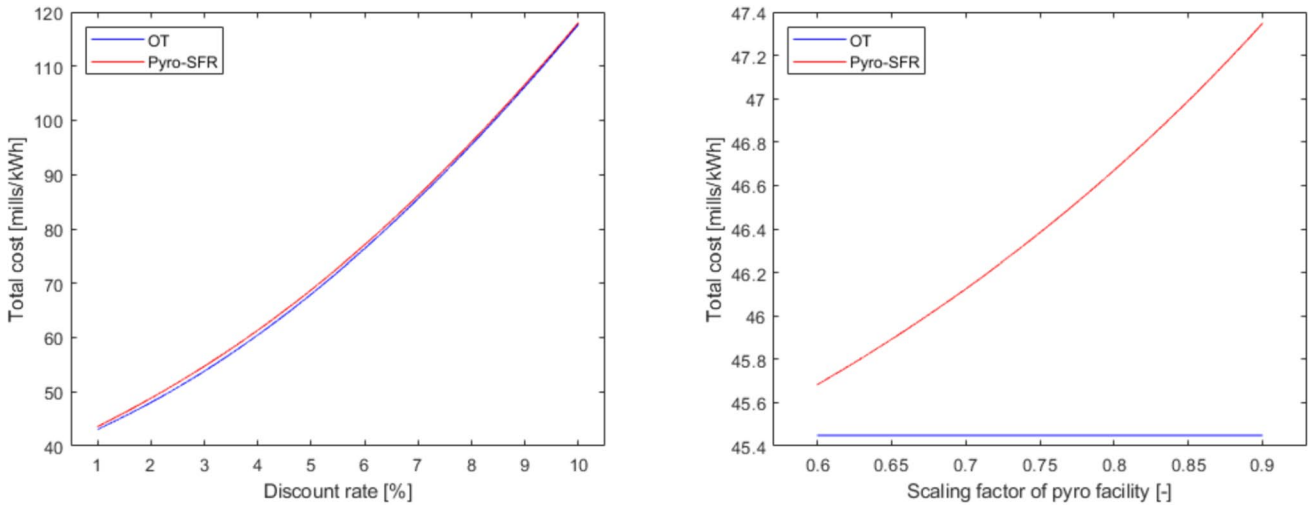


**Fig. 18** Sensitivity analysis for the discount rate and the scaling factor of pyro-processing facility

low nonlinearity of the model, employing low and high values sufficed to capture the full sensitivity spectrum. Total and fuel cycle costs were computed using the low and high values of the unit cost for one module while maintaining the mode values for the other modules. Subsequently, the modules were ranked based on their impact on the cost, generating tornado diagrams as depicted in Figs. 14 and 15. In the tornado diagrams, the relative influence of cost is represented by the width of the bars. The value displayed above the centerline denotes the cost when all modules are set to the mode value of the unit cost. Regarding total cost sensitivity, the PWR capital cost emerged as the most influential factor for both cycles. Concerning fuel cycle cost, NU mining cost exhibited the highest sensitivity for both cycles.

A break-even point analysis was conducted on the sensitive modules identified from the tornado diagrams. This analysis involves determining whether there exists a unit cost point within the range where the total costs of the pyro-SFR and OT cycles are equal. Figure 16 presents the results of the break-even point analysis for the unit costs of PWR and SFR capital, which contribute significantly to the total cost. In summary, the pyro-SFR cycle becomes economically advantageous when the unit cost of SFR capital is less than approximately 0.9 times the unit cost of PWR capital. However, it is anticipated that in the near future, the unit cost of SFR capital will not be lower than that of PWR capital. This expectation stems from the higher technical maturity of PWR compared to SFR, along with a greater wealth of experience in constructing commercial-scale reactors. The mean value of the unit cost of SFR capital in AFC-CBR in Table 4 is approximately 1.07 times the mean value of the unit cost of PWR capital, indicating a rather optimistic outlook. The break-even point analysis depicted in Fig. 16 illustrates the widening cost gap between the two options as the unit cost of SFR capital increases.

Figure 17 illustrates the results of a break-even point analysis conducted on the most sensitive fuel cycle module, NU mining, and the most interesting fuel cycle module, pyro-processing. When the unit cost of NU mining exceeds 314 $/kgU, the total cost of the pyro-SFR cycle becomes economically favorable. No break-even point was identified for the pyro-processing unit cost.

The discount rate plays a crucial role in determining the total cost as it influences the calculation of the IDC and CRF values in the reactor capital, and presents values of all costs. Figure 18 depicts the variations in the total costs of the pyro-SFR and OT cycles as the discount rate escalates from 1 to 10%. As a result, there is no significant alteration in the difference between the total costs of the two options, with both witnessing an increase due to the increasing IDC and CRF values.

Considering economies of scale, parameters that affect costs are the capacity size and the scaling factor of the reference facility. Reliable estimation of the scaling factor is challenging with insufficient data, as the scaling factor is typically derived from regression analysis of unit cost data across multiple capacity sizes. The scaling factor for the unit costs based on the pyro-processing reference facility in Table 5 was derived from only two capacities: 20 ton/y and 200 ton/y [21]. Therefore, it is necessary to conduct additional sensitivity analysis on this scaling factor, which has low reliability, but is applied across several unit costs. When the scaling factor varies from 0.6 to 0.9, a range commonly used for chemical processes, the total cost changes as shown in Fig. 18. Given that the average mass flow of pyro-processing is approximately 700 ton/y in the current scenario, the unit costs could potentially be lower than the

values in Table 4 if the economies of scale is considered. However, a higher scaling factor reduces the extent to which unit costs can decrease. Consequently, as the scaling factor increases, the cost gap between the pyro-SFR cycle and OT cycle widens.

## Conclusion

In this study, a comparative and quantitative system analysis was undertaken to assess the transition scenarios to fuel cycle options: the OT and pyro-SFR cycles. Initially, the fuel cycle system was delineated using flow diagrams based on the INL module concept. Subsequently, a dynamic mass-flow model, incorporating reasonable logic for transportation and facility operation, was formulated, assuming static and continuous states for each time step. By resolving the mass-flow model while reflecting current Korean nuclear plans in the transition scenarios, the mass flows for all modules were determined, enabling comparisons of quantitative factors such as resource requirement and waste generation. An economic evaluation model was developed, incorporating detailed equations for calculating the IDC in the reactor capital cost and the optimal concentration of DU. Unit costs tailored to the scale of the Korean nuclear system were applied to derive LCOE values for comparing the economic feasibility of the fuel cycle options. To address uncertainties in unit costs, an uncertainty analysis was conducted via a Monte Carlo simulation, and a sensitivity analysis was conducted to identify the most sensitive modules and their break-even points.

The system analysis utilizing enhanced models revealed several insights into potential fuel cycle options in Korea. In the mass-flow analysis, the pyro-SFR cycle demonstrated advantages over the OT cycle concerning resource requirement and HLW generation per unit of electricity generated. Compared to the OT cycle, the pyro-SFR cycle necessitates smaller capacities for interim storage and disposal facilities for spent fuel but entails additional facilities, including the SFR, pyro-processing facility, and storage and disposal facilities for radioactive waste from pyro-processing. In the economic analysis, the LCOE of total cost for the pyro-SFR cycle (46.06 mills/kWh) was estimated to be slightly higher than that for the OT cycle (45.45 mills/kWh). The increase in cost stemming from the construction and operation of SFRs and additional facilities for the pyro-SFR cycle was largely offset by the additional electricity generation. Moreover, considering the uncertainties in unit costs, the cost gap between the two options was not significant, as the standard deviation of the cost distribution exceeded the cost gap. Finally, break-even points were identified in the unit costs of the sensitive modules, including reactor capital and NU mining.

This paper presented a well-structured calculation formula for mass-flow analysis and economic evaluation, including the IDC calculation of reactor capital, optimal DU concentration, and economies of scale for the unit cost, which were not clearly addressed in the previous studies. Notably, applying economies of scale reduced the cost difference between the pyro-SFR cycle cost and the OT cycle compared to the previous studies. This result was derived by applying scaling factors from AFC-CBR 2017 [21], necessitating further analysis of their validity for more reliable results. Additionally, since AFC-CBR 2017 provides unit costs based on US data, it is necessary to convert these into unit costs for Korea. This requires comparing and analyzing the detailed components of the unit cost for each module to identify differences or ratios between unit costs in the US and Korea. More meaningful results could be achieved by applying Korean unit costs in future studies.

The system analysis methodology presented furnishes valuable evaluation criteria for decision-making in spent fuel management plans or policies. However, evaluating future fuel cycle options is challenged by limited data in the current scenario, where not all fuel cycle technologies have been commercialized. Hence, ongoing efforts to reduce uncertainty and enhance the accuracy of evaluation criteria are imperative, necessitating the refinement of models and the acquisition of reliable data.

**Acknowledgements** This work was supported by the National Research Foundation of Korea (NRF) grant funded by the Korea government (MSIT) (No. 2021M2E3A1040058).

## References

1. IAEA, "Planning Enhanced Nuclear Energy Sustainability: An INPRO Service to Member States, Analysis Support for Enhanced Nuclear Energy Sustainability (ASENES), IAEA Nuclear Energy Series, No. NG-T-3.19," IAEA, 2021.
2. IAEA, "Framework for Assessing Dynamic Nuclear Energy Systems for Sustainability: Final Report of the INPRO Collaborative Project GAINS, IAEA Nuclear Energy Series, No. NP-T-1.14," IAEA, 2013.
3. IAEA, "Enhancing Benefits of Nuclear Energy Technology Innovation through Cooperation among Countries: Final Report of the INPRO Collaborative Project SYNERGIES, IAEA Nuclear Energy Series, No. NF-T-4.9," 2018.
4. IAEA, "Application of Multi-criteria Decision Analysis Methods to Comparative Evaluation of Nuclear Energy System Options: Final Report of the INPRO Collaborative Project KIND, IAEA Nuclear Energy Series, No. NG-T-3.20," 2019.
5. IAEA, "Comparative Evaluation of Nuclear Energy System Options: Final Report of the INPRO Collaborative Project CENESO, IAEA-TECDOC-2027," 2023.
6. W.I. Ko, H. Choi, M.S. Yang, Economic analysis on direct use of spent pressurized water reactor fuel in CANDU reactors-IV: DUPIC fuel cycle cost. Nucl. Technol. **134**(2), 167–186 (2001)

7. W.I. Ko, H.D. Kim, M.S. Yang, Advantages of irradiated DUPIC fuels from the perspective of environmental impact. Nucl. Technol. **138**(2), 123–139 (2002)
8. W.I. Ko, F. Gao, Economic analysis of different nuclear fuel cycle options. Sci. Technol. Nuclear Install. **2012**, 1–10 (2012)
9. B.H. Park, F. Gao, E.-H. Kwon, W.I. Ko, Comparative study of different nuclear fuel cycle options: quantitative analysis on material flow. Energy Policy **39**, 6916–6924 (2011)
10. F. Gao, W.I. Ko, Modeling and system analysis of fuel cycles for nuclear power sustainability (I): uranium consumption and waste generation. Ann. Nucl. Energy **65**, 10–23 (2014)
11. F. Gao, W.I. Ko, Modeling and system analysis of fuel cycles for nuclear power sustainability (III): an integrated evaluation. Prog. Nucl. Energy **74**, 79–90 (2014)
12. S. Yoon, S. Choi, W.I. Ko, An integrated multicriteria decision-making approach for evaluating nuclear fuel cycle systems for long-term sustainability on the basis of an equilibrium model: technique for order of preference by similarity to ideal solution, preference ranking organiz. Nucl. Eng. Technol. **49**, 148–164 (2017)
13. R. Gao, S. Choi, Y. Zhou, W.I. Ko, Performance modeling and analysis of spent nuclear fuel recycling. Int. J. Energy Res. **39**, 1981–1993 (2015)
14. R. Gao, S. Choi, W.I. Ko, S. Kim, Economic potential of fuel recycling options: a lifecycle cost analysis of future nuclear system transition in China. Energy Policy **101**, 526–536 (2017)
15. R. Gao, H.O. Nam, W.I. Ko, H. Jang, Integrated system evaluation of nuclear fuel cycle options in China combined with an analytical MCDM framework. Energy Policy **114**, 221–233 (2018)
16. R. Gao, H.O. Nam, W.I. Ko, H. Jang, National options for a sustainable nuclear energy system: MCDM evaluation using an improved integrated weighting approach. Energies **10**, 1–24 (2017)
17. S. Choi, W.I. Ko, Dynamic assessments on high-level waste and low- and intermediate-level waste generation from open and closed nuclear fuel cycles in Republic of Korea. J. Nucl. Sci. Technol. **51**(9), 1141–1153 (2014)
18. S. Choi, H.J. Lee, W.I. Ko, Dynamic analysis of once-through and closed fuel cycle economics using monte carlo simulation. Nucl. Eng. Des. **277**, 234–247 (2014)
19. F. Gao, W.I. Ko, Dynamic analysis of a pyroprocessing coupled SFR fuel recycling. Sci. Technol. Nuclear Install. **2012**, 1–10 (2012)
20. S. Abousahl, P. Carbol, B. Farrar, H. Gerbelova, R. Konings, K. Lubomirova, M. Martin Ramos, V. Matuzas, K. Nilsson, P. Peerani, M. Peinador Veira, V. Rondinella, A. Van Kalleveen, S. Van Winckel, J. Vegh and F. Wastin, Technical assessment of nuclear energy with respect to the 'do no significant harm' criteria of Regulation (EU) 2020/852 ('Taxonomy Regulation'), Luxembourg: Publications Office of the European Union, 2021.
21. B. Dixon, F. Ganda, E. Hoffman, J. Hansen, E. Schneider, D. Shropshire and K. Williams, Advanced Fuel Cycle Cost Basis - 2017 Edition, INL/EXT-17–43826, Idaho National Laboratory, 2017.
22. J.M.A. Williamson, Pyroprocessing flowsheets for recycling used nuclear fuel. Nucl. Eng. Technol. **43**(4), 329–334 (2011)
23. Ministry of Trade, Industry & Energy, "The 10th Basic Plan on Electricity Demand and Supply (2022~2036)," Ministry of Trade, Industry & Energy, Seoul, 2023.
24. Ministry of Trade, Industry & Energy, "Basic Plan on High-level Radioactive Waste Management(Draft)," Ministry of Trade, Industry & Energy, Seoul, 2016.
25. Ministry of Trade, Industry & Energy, "The 2nd Basic Plan on High-level Radioactive Waste Management," Ministry of Trade, Industry & Energy, Seoul, 2021.
26. Organization for Economic Co-operation and Development, National Accounts: National Accounts Deflators: Gross Domestic Product: GDP Deflator for United States [USAGDPDEFQISMEI], retrieved from FRED, Federal Reserve Bank of St. Louis; https://fred.stlouisfed.org/series/USAGDPDEFQISMEI, June 27, 2024.
27. Ministry of Trade, Industry & Energy, Regulations on the calculation standards of radioactive waste management cost and spent nuclear fuel management charge, Notice no. 2022–11, Republic of Korea, 2022.
28. S.L. Savage, *The Flaw of Averages: Why We Underestimate Risk in the Face of Uncertainty* (Sohn Wiley & Sons, 2009)